Progressive Collapse Analysis on Multicore Computers Using Nonlinear Dynamic Approach

Sergiy FIALKO

Cracow University of Technology, Kraków, Poland; e-mail: sergiy.fialko@gmail.com

A method for solving the problem of structural progressive destruction is proposed, based on nonlinear finite element dynamic analysis, taking into account both physical and geometrical nonlinearity. Unlike most existing approaches, a specialized method has been implemented to simulate the sudden removal of groups of finite elements at given times, which makes it possible to simulate not only the removal of columns but also fragments of load-bearing walls and staircase-elevator blocks. The proposed approach involves the numerical integration of the Cauchy problem using an implicit method of the predictor-corrector type, with multithreaded parallelization of all key algorithms to accelerate the solution. The reliability of the numerical results is substantiated by comparison with the experimental results presented in other studies. The behavior of realistic structural models with bearing walls as well as without them, consisting of exclusively nonlinear finite elements, under the sudden removal of a fragment of a staircase-elevator block, is studied.

Keywords: progressive collapse analysis, nonlinear dynamic analysis, finite element method, Cauchy problem, multithreaded parallelization.

1. Introduction

The progressive destruction problem of multi-story building structures due to the explosions of domestic gas, collisions of a road train, projectile impact, or sabotage act is considered. In the first stage, a nonlinear static problem is solved under the action of dead and live loads. This solution provides the initial displacements and the stress-strain state of the nonlinear finite elements, which are used as the initial conditions for the next stage. In the second stage, the integration of nonlinear equations of motion is conducted, where the initiating action is caused by the sudden removal of a group of finite elements according to the chosen failure scenario, with each finite element being removed at a designated time.

A classic example of progressive collapse is the destruction of the World Trade Center Twin Towers as a result of the terrorist attack of September 11, 2001. A detailed analysis of this disaster is presented in [1]. The studies in [2–4] give the problem formulations of progressive collapse analysis and provide a review of articles devoted to this problem. It is emphasized that in the problems of progressive destruction, it is typical that a small initial local destruction of the load-bearing elements of the structure leads to disproportionately large destruction of its significant parts. To nullify the internal forces in the removed column, both the application of a nodal load of the appropriate value and the replacement of the removed column with its reactions are used, which are instantly nullified at the time of removal. In many works, it is noted that to obtain more reliable results from the simulation, it is important to take into account the dynamic response of the structure after the removal of the selected elements.

In [5], the dynamic behavior an 8-story steel frame of building is considered when a column of the lower floor is suddenly removed. The calculation model consists of spatial frame finite elements. The non-linear properties of the material are taken into account. An explicit method for integrating nonlinear equations of motion is used, implemented in the LS-DYNA software.

In [6], the dynamic behavior of the design model of a 20-story building, consisting of a steel frame finite elements and reinforced concrete floor slabs (quadrilateral shell elements), is analyzed following the sudden removal of a corner column on the first floor. Physical nonlinearity is taken into account for both frame finite elements and shell ones. The nonlinear dynamic analysis was performed using the ABAQUS FEA software.

In [7], the simulation of the destruction process of a 6-story frame building, consisting of reinforced concrete columns with rectangular sections, reinforced concrete rectangular beams, and floor slabs, is presented. Volumetric finite elements are used to model the behavior of concrete for beams, columns, and floor slabs. The nonlinear properties of concrete and reinforcement are taken into account. To simulate the initiating action, the LOAD_BLAST module of the LS-DYNA program is used, which simulates the explosive action of a non-contact TNT charge with a mass of 500 kg, destroying the corner column of the first floor. The integration of nonlinear equations of motion is carried out by the explicit method within the same software package.

The reinforced concrete frame of a 3-story building is considered in [8]. One of the lower floor columns is suddenly removed. For comparison with the results of the experiment, both linear and nonlinear dynamic analysis are performed, and for the nonlinear analysis, an approximate model is used in which all the elasto-plastic properties of the material are realized by so-called nonlinear hinges, the locations of which along the length of each spatial frame finite elements are

set *a priori*. The rest of the rod behaves elastically. The SAP-2000 software is used for the analysis.

The influence of the speed of column removal for the spatial asymmetrical frame model on its behavior is considered in [9].

The experimental results are compared with the results obtained by the finite element method using the LS-DYNA software [10]. The strength of the connections of beams with columns is investigated for both steel and reinforced concrete beams and columns, with the load applied statically.

The simplified calculation model based on the consideration of only the section of a multi-story building that is adjacent to the instantly removed column is used [11]. The action of the remaining structure is replaced by elastic springs. Nonlinear static analysis is performed and dynamic effects are taken into account based on dynamic amplification factors.

In the analysis of progressive collapse, both static linear and nonlinear approaches are widely used in [12–17] and others. The main focus of this research is to determine and clarify the dynamic amplification (increase) factor, which is used to increase the values of internal forces obtained from static analysis. Static approaches are much easier and less-time consuming than linear or nonlinear dynamic analysis.

The list of works devoted to this problem can be easily extended. However, we will restrict ourselves to the above-mentioned works and refer to articles [2–4], containing extensive reviews.

The considered studies highlight the following features:

- There are practically no works in which fragments of load-bearing walls are instantly removed. In modern calculation models of multi-story buildings, often the supporting structures include often not only columns, but also the walls of staircase-elevator blocks and simple walls. Therefore, methods of the numerical analysis of progressive collapse should be able to include the removal of not only columns but also fragments of load-bearing walls in the failure scenario.

- In many computational models, to reduce the time of numerical analysis, simplified models are used – lumped plasticity, the behavior of individual fragments of structure, taking into account physical nonlinearity, or the ultimate simplification of the computational model. As a rule, real calculation models are much more complicated. There are no regular geometric shapes, and there are various types of finite elements (triangular and quadrilateral finite elements of plates and shells, spatial frame finite elements, rigid connections, elastic supports, elastic foundation, unilateral connections, etc.). These features can lead to significant deviations in the behavior of the actual computational model compared to the simplified one.

This work aims to develop a numerical method for analyzing the progressive destruction of multi-story building structures, as well as structures of arbitrary types, based on nonlinear dynamic analysis of the entire design model, taking into account both geometric nonlinearity and the elasto-plastic properties of the material. The destruction of concrete and reinforcement, as well as the materials used in metal structures, is modeled using a damage parameter.

Distinctive features of the proposed method are:

- Development of a new approach that implements instant removal of finite elements of any type at specified points in time. Unlike classical approaches, the proposed method does not require any preliminary information about the internal forces in the removed finite elements, which allows to remove not only spatial frame finite elements but also plate finite elements of load-bearing walls and staircase-elevator blocks, as well as finite elements of any arbitrary types. This is very important in the analysis of the progressive destruction of modern multi-story buildings.

- Original multithreaded parallelization algorithms, covering all principal stages of the solution method: assembling a sparse matrix, its factorization, performing forward and backward substitutions, calculating the vector of internal forces, have been developed that make it possible to analyze computational models of the order of $200\,000$–$1\,500\,000$ nonlinear algebraic equations on modern multi-core computers of the Symmetric Multiprocessing (SMP) and Non-Uniform Memory Access (NUMA) architecture in a time frame acceptable for designers.

- Unlike most approaches implemented in modern software systems, in the proposed method both frame and shell finite elements are considered volumetric bodies, to which the corresponding static and kinematic hypotheses of bars, plates, and shells of medium thickness are successively applied. This makes it possible to more strictly formulate the elasto-plastic problem, as well as to simplify obtaining resolving relations and their numerical implementation in software code.

- For a spatial frame finite element, taking into account geometric nonlinearity in the Taylor series expansion, up to sixteen terms of the series are retained to approximate the longitudinal strain, which allows modeling the initial post-buckling behavior using only the initial configuration of the structure. In contrast to the traditional approach, based on total Lagrangian formulation with retaining only the first two terms of Tailor series expansion, the proposed method describes the post-buckling behavior of the rod, while the conventional method does not allow exceeding the value of the critical buckling load.

2. Finite element library

The developed library of finite elements, which simultaneously takes into account the geometric nonlinearity and the elasto-plastic properties of the material, includes a two-node finite element of the spatial frame, as well as isoparametric triangular and quadrilateral flat shell finite elements. When modeling the behavior of reinforced concrete structures, these finite elements contain inclusions that represent the reinforcement. In this case, both concrete and reinforcement use their respective material models based on the theory of plastic flow. The compatibility of concrete and reinforcement is ensured by the kinematic coupling conditions. In the case of a homogeneous material, there are no inclusions, and, when it comes to metal structures, the von Mises yield criterion and the kinematic hardening model are used. In this paper, we will restrict ourselves to the consideration of reinforced concrete structures.

For a spatial frame finite element, the shear model of S.P. Timoshenko is used, while the Mindlin–Reissner model is implemented for shell finite elements. All types of finite elements ensure the absence of shear locking. The shape functions of the shell finite elements are compatible with the shape functions of the spatial frame finite element, which guarantees the compatibility of displacements between floor slabs and stiffening ribs not only at the nodes but also along the entire interface line. The work of the reinforcement is considered not only in tension-compression but also in transverse shear, which ensures the stability of the computational algorithm even if the concrete in the finite element is completely destroyed [18]. In shell finite elements, the direction of the reinforcing rods can be rotated by an arbitrary angle relative to the axis of the local coordinate system normal to the middle surface, which allows for the modeling of non-orthogonal reinforcement and structures of complex geometry.

Accounting for geometric non-linearity is essential when it comes to large displacements and angles of rotation. In conventional normative analysis, reinforced concrete structural elements are quite stiff, so taking into account geometric nonlinearity may lead to confusion for the reader. However, with progressive destruction, as well as with strong seismic action, often referred to as extreme impacts, partial destruction of supporting structures is allowed, which causes large displacements and rotations. Therefore, for these types of analyses, it may be necessary to take into account geometric nonlinearity.

A complete accounting of geometric nonlinearity includes consideration of large displacements, large rotation angles and large strains. This is achieved, for example, by recalculating the coordinates of the nodes of the finite element model at the end of each converged load step (updated Lagrangian formulation). On the other hand, the updated Lagrangian formulation approach usually leads to more iterations when using the Newton–Raphson method and more calcula-

tion failures due to a lack of convergence compared to the methods based on the total Lagrangian formulation and retaining a lot of terms in Taylor series expansion of strains, used in the proposed approach. A similar conclusion was also made in [19, p. 423], when comparing the updated Lagrangian formulation approach with the $P - \Delta$ analysis. Taking into account this fact, as well as the fact that we are dealing with building structures, and not with fragments of aircraft, satellite antennas, and other flexible structures, we use a Taylor series expansion of strains in the Cauchy relations connecting strains with derivatives of displacements, which refer to the initial configuration. Our approach, like the classical one, is based on the total Lagrangian formulation, but if the classical method uses the Cauchy–Green tensor with the quadratic approximation of the nonlinear part [20, Section 11.8], then we propose a novel algorithm that makes it possible to retain any number of terms of the series in the Taylor expansion. For a spatial frame finite element, the quadratic approximation does not allow describing post-buckling behavior; therefore, to overcome this shortcoming, we increase the number of terms in the Taylor series expansion to 16, refining the behavior of the calculation model. In contrast, for shell finite elements, the classical quadratic approximation will allow us to simulate initial post-buckling behavior, so we limit ourselves to the classical total Lagrangian formulation. The proposed approach is more limited in terms of displacements and rotation angles than the updated Lagrangian formulation, but, as mentioned above, in many cases it requires a smaller number of iterations of the Newton–Raphson method, and significantly less often leads to divergence of the iterative process. A comparison of these approaches using a simple problem, having an exact analytical solution, as an example is given in Subsec. 3.1.

2.1. Material models

In this formulation of the problem, we do not consider structural elements consisting only of concrete, since reinforced concrete is usually used in real structures. Therefore, we neglect the initial anisotropy of concrete in comparison with the structural anisotropy due to the presence of reinforcement. The behavior of concrete is described using the plastic flow theory, and the flow surface is taken in the form of a non-circular paraboloid, as proposed in [21], defined as the strength surface:

$$f = 3\overline{\alpha}^2 b I_1 + \frac{3\sqrt{3}}{2}\beta \left(a - b I_1\right) J_3 J_2^{-\frac{3}{2}} + 3J_2 - \sigma_0, \tag{1}$$

where $a = \overline{\sigma_c \sigma_t}$, $b = \overline{\sigma_c} + \overline{\sigma_t}$, $\beta = 1 - 3\overline{\alpha}^2$, $\sigma_0 = 3a\overline{\alpha}^2$, $\overline{\alpha} \in \left(0.531, \sqrt{3}\right]$. Here $\overline{\alpha}$ is a parameter that specifies the deviation of the paraboloid from the circular shape. At $\overline{\alpha} = 0.531$, the paraboloid has a maximum deviation, and

at $\overline{\alpha} = \sqrt{3}$ it becomes circular. Parameters I_1, J_2, and J_3 are respectively the first invariant of the stress tensor, as well as the second and third invariants of the stress deviator. As plastic deformations develop, the yield surface moves in the space of principal stresses and expands in the case of isotropic hardening or contracts in the case of softening. The parameters $\overline{\sigma_c}$ and $\overline{\sigma_t}$ change as follows:

$$\overline{\sigma}_t = \begin{cases} \sigma_t + H_t \varepsilon_{ps}, \sigma_t + H_t \varepsilon_{ps} > \alpha \sigma_t, \\ \\ \alpha \sigma_t, \sigma_t + H_t \varepsilon_{ps} \leq \alpha \sigma_t, \end{cases} \qquad t \leftrightarrow c, \qquad (2)$$

where ε_{ps} is a measure of plastic strain, $H_t = E_t/(1 - E_t/E)$, E is an initial deformation modulus for concrete, the parameter $\alpha \in [0, 1]$ determines the residual strength of concrete, and σ_c and σ_t are the initial compressive and tensile strength of concrete, respectively.

Figure 1a shows a typical diagram $\sigma - \varepsilon$ for concrete (solid line), while in Fig. 1b depicts the dependence of the damage parameter p on the reduced strain ε. Usually, the parameter $d = 1 - p$ is taken as the damage parameter, where $d = 0$ denotes an intact structural element and $d = 1$ signifies a completely destroyed one. It is more convenient for us to use the parameter p when $p = 1$ corresponds to an undamaged structural element and $p = 0$ denotes a completely destroyed one. The onset of concrete destruction is usually associated
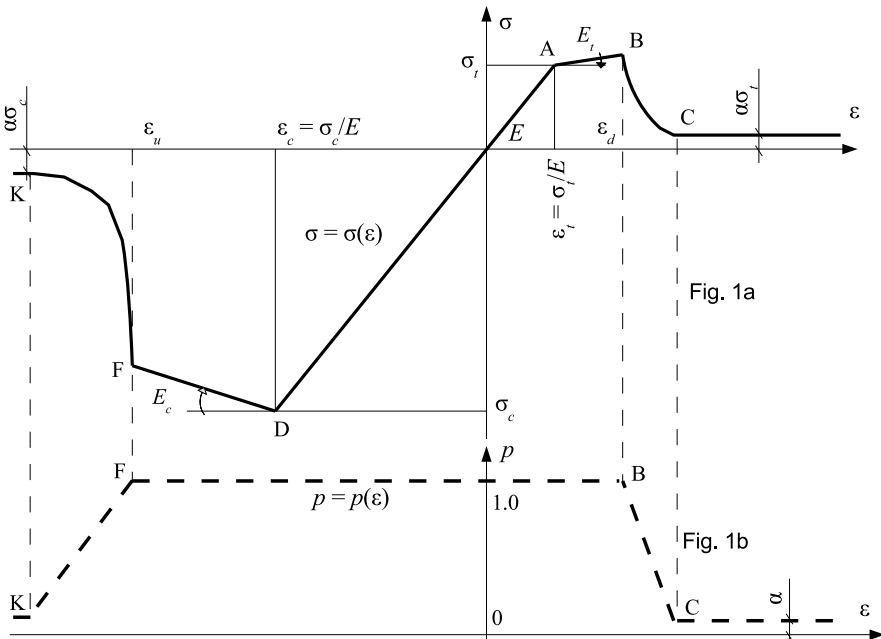

FIG. 1. a) $\sigma - \varepsilon$ diagram, b) the damage parameter $p = p(\varepsilon)$ for concrete.

with the value of fracture energy G_f. However, in most design codes, ultimate deformations are given, above which destruction begins.

Therefore, the proposed approach assumes that $p = p(\varepsilon)$ – Fig. 1b. In Fig. 1a, E_t and E_c are the modules of strengthening and/or softening of concrete in the tension and compression zones, respectively. If $E_t > 0$ $(t \leftrightarrow c)$, then the yield surface expands (isotropic hardening). If $E_t < 0$ $(t \leftrightarrow c)$, then the yield surface is compressed. Details are given in [18]. Points A, B, and C correspond to the beginning of the plastic flow, the beginning and the end of the destruction of concrete in the tension zone. The parameter ε_t is the strain corresponding to the onset of plastic flow in tensile concrete, while ε_d is the strain at which concrete tensile cracking begins (usually $\varepsilon_d = \varepsilon_t$ and points A and B coincide). Points D, F, and K correspond to the beginning of the plastic flow, the beginning and the end of the destruction of concrete in the compressed zone. The parameter ε_c is the strain corresponding to the beginning of the concrete flow in compression, and ε_u is the strain at which the destruction of concrete begins in compression.

The analysis of the steel is described by the von Mises plastic flow theory with kinematic hardening, which takes into account the Bauschinger effect for steel, an essential consideration for the dynamic behavior of the structure. A bilinear diagram $\sigma - \varepsilon$ is used.

2.2. Spatial frame finite element

The spatial frame finite element (Fig. 2) can have a cross-section of arbitrary shape containing holes and cutouts. The cross-section is triangulated, resulting in the spatial frame being divided into separate triangular prisms. One Gauss point along length is used in the calculation of quadratures via the Gauss–Legendre method from the finite element volume. As a result, the components of the stress
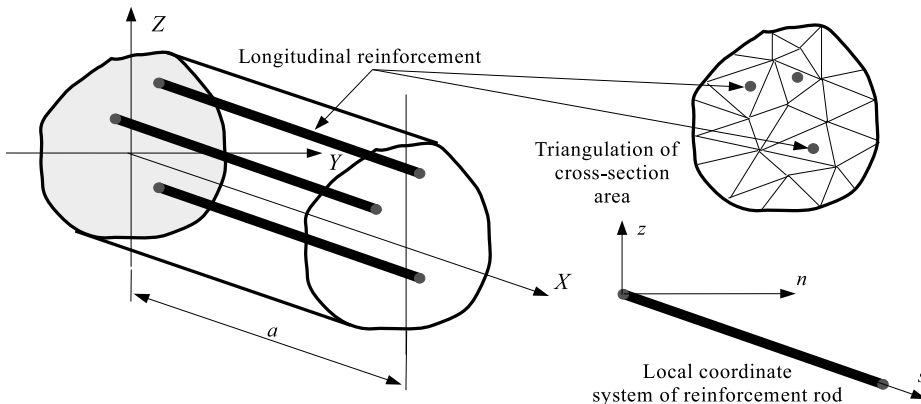

Fig. 2. Spatial frame finite element.

and strain tensors are determined at the centers of gravity of each triangular prism.

Longitudinal reinforcement is considered discretely, and the centers of gravity of reinforcing rods may not coincide with the triangulation vertices. To obtain the tangent stiffness matrix of the finite element and the vector of internal forces, the principle of the virtual works is used:

$$\iiint\limits_{V} \boldsymbol{\sigma}_c \colon \boldsymbol{\varepsilon}_c dV + \sum_s A_s \int\limits_0^a \boldsymbol{\sigma}_s \colon \boldsymbol{\varepsilon}_s dx - \delta A_{\text{ext}} = 0, \tag{3}$$

where

$$\boldsymbol{\sigma}_c = \begin{pmatrix} \sigma_x & \tau_{xy} & \tau_{xz} \\ \tau_{yx} & 0 & 0 \\ \tau_{zx} & 0 & 0 \end{pmatrix}, \qquad \boldsymbol{\varepsilon}_c = \begin{pmatrix} \varepsilon_x & 0.5\gamma_{xy} & 0.5\gamma_{xz} \\ 0.5\gamma_{yx} & -\nu\varepsilon_x & 0 \\ 0.5\gamma_{zx} & 0 & -\nu\varepsilon_x \end{pmatrix}, \tag{4}$$

$$\boldsymbol{\sigma}_s = \begin{pmatrix} \sigma_s & \tau_{sn} & \tau_{sz} \\ \tau_{ns} & 0 & 0 \\ \tau_{zs} & 0 & 0 \end{pmatrix}, \qquad \boldsymbol{\varepsilon}_s = \begin{pmatrix} \varepsilon_s & 0.5\gamma_{sn} & 0.5\gamma_{sz} \\ 0.5\gamma_{ns} & -\nu_s\varepsilon_s & 0 \\ 0.5\gamma_{zs} & 0 & -\nu_s\varepsilon_s \end{pmatrix}. \tag{5}$$

Here $\boldsymbol{\sigma}_c$ and $\boldsymbol{\varepsilon}_c$ are the stress and strain tensors, taking into account all static and kinematic hypotheses of the theories of Kirchhoff–Clebsch bars and S.P. Timoshenko, $\boldsymbol{\sigma}_s$ and $\boldsymbol{\varepsilon}_s$ are the stress and strain tensors for the reinforcing rod s considering the work not only in tension-compression but also in transverse shear, and ν and ν_s are the Poisson's ratios for the materials of the spatial frame finite element and the reinforcement, respectively. The directions of the axes s, n, z are shown in Fig. 2, with the s, n and z axes being parallel to the OX, OY and OZ axes, respectively. In (3), summation over s covers all rods of longitudinal reinforcement, A_s is the cross-sectional area of the s-th rod, A_{ext} is the work of external forces, and V is the volume of the entire bar.

The kinematic coupling conditions of the reinforcing rods and concrete ensure the absence of slippage:

$$\varepsilon_s = \varepsilon_x, \qquad \gamma_{sn} = \gamma_{xy}, \qquad \gamma_{sz} = \gamma_{xz}. \tag{6}$$

The longitudinal deformation of a fiber parallel to the central axis of a spatial frame finite element is represented as follows:

$$\varepsilon_x\left(x, y, z\right) = \sqrt{1 + A^2} - 1, \tag{7}$$

where

$$A^2 = 2\left[\frac{\partial \acute{u}}{\partial x} + \frac{1}{2}\left(\frac{\partial \acute{u}}{\partial x}\right)^2 + \frac{1}{2}\left(\frac{\partial v}{\partial x}\right)^2 + \frac{1}{2}\left(\frac{\partial w}{\partial x}\right)^2\right], \tag{8}$$

$\acute{u} = \acute{u}(x, y, z)$, $v = v(x)$ and $w = w(x)$, where $\acute{u}$, v, and w are displacements of arbitrary point of finite element. Let us expand the expression $\sqrt{1 + A^2}$ in a Taylor series:

$$\varepsilon_x(x, y, z) = \frac{\partial \acute{u}}{\partial x} + \frac{1}{2}\left(\frac{\partial v}{\partial x}\right)^2 + \frac{1}{2}\left(\frac{\partial w}{\partial x}\right)^2 - \frac{1}{2}\left[\frac{1}{2}\left(\frac{\partial v}{\partial x}\right)^2 + \frac{1}{2}\left(\frac{\partial w}{\partial x}\right)^2\right]^2$$

$$+ \frac{1}{2}\left[\frac{1}{2}\left(\frac{\partial v}{\partial x}\right)^2 + \frac{1}{2}\left(\frac{\partial w}{\partial x}\right)^2\right]^3 - \frac{5}{8}\left[\frac{1}{2}\left(\frac{\partial v}{\partial x}\right)^2 + \frac{1}{2}\left(\frac{\partial w}{\partial x}\right)^2\right]^4 + \ldots \tag{9}$$

Here, we assume that $\acute{u} \ll v$, $\acute{u} \ll w$ and $\left(\frac{\partial \acute{u}}{\partial x}\right)^2 \ll \frac{\partial \acute{u}}{\partial x}$, based on which in Eq. (9) we retain only the term $\frac{\partial \acute{u}}{\partial x}$, which occurs in the first degree. Usually, for a rod in the Taylor expansion, only the first two terms of the series are retained: $\varepsilon_x(x, y, z) = \frac{\partial \acute{u}}{\partial x} + \frac{1}{2}\left(\frac{\partial v}{\partial x}\right)^2 + \frac{1}{2}\left(\frac{\partial w}{\partial x}\right)^2$. However, this conventional approach does not allow one to simulate the post-buckling behavior of a compressed rod, since in the presence of a small eccentricity, initial imperfection, or a small transverse load, the transversal displacements of the compressed rod tend to infinity as the value of the longitudinal compressive force tends to the critical one, corresponding to the loss of stability of an ideal elastic rod (see Subsec. 3.1). In addition, the quadratic approximation of longitudinal deformation is acceptable as long as the change in the geometry of the structure is negligible. It is usually assumed that $w/h < 2, w \leftrightarrow v$, where h is the height of characteristic section. However, when analyzing progressive collapse, the displacements of structural elements can be so large that the shape of the deformed system changes significantly. Therefore, we propose an algorithm based on a total Lagrangian formulation that allows us to keep the arbitrary number of terms of Tailor series expansion, which makes it possible to describe the initial post-buckling behavior of an individual rod of a spatial frame, and take into account significant changes in its initial geometry. In practice, we keep up to 16 terms.

Expressing the longitudinal displacement of the fiber $\acute{u}(x, y, z)$ through the longitudinal displacement of the central axis of the rod $u(x)$ and using the hypothesis of direct normals, we obtain: $\acute{u}(x, y, z) = u(x) + y \cdot \beta_y(x) + z \cdot \beta_z(x)$, where $\beta_y = -\theta_z$, $\beta_z = \theta_y$, θ_y, θ_z are the rotation angles of the normal to the central axis relative to the axes OY and OZ, due to the bending of the rod.

Finally, we obtain:

$$
\begin{cases}
\varepsilon_x = \varepsilon_x^{\text{lin}} + \varepsilon_x^{\text{nonlin}}, \\
\gamma_{xy} = \beta_y \dfrac{\partial v}{\partial x} - z \dfrac{\partial \theta_x}{\partial x}, \\
\gamma_{xz} = \beta_z \dfrac{\partial w}{\partial x} + y \dfrac{\partial \theta_x}{\partial x},
\end{cases}
\tag{10}
$$

where θ_x is the torsion angle of the rod, $\varepsilon_x^{\text{lin}}$ and $\varepsilon_x^{\text{nonlin}}$ are the linear and non-linear components of the longitudinal strain, respectively:

$$
\begin{aligned}
\varepsilon_x^{\text{lin}} &= \frac{\partial u}{\partial x} + y \frac{\partial \beta_x}{\partial x} + z \frac{\partial \beta_z}{\partial x}, \\
\varepsilon_x^{\text{nonlin}} &= \frac{1}{2}\left(\frac{\partial v}{\partial x}\right)^2 + \frac{1}{2}\left(\frac{\partial w}{\partial x}\right)^2 - \frac{1}{2}\left[\frac{1}{2}\left(\frac{\partial v}{\partial x}\right)^2 + \frac{1}{2}\left(\frac{\partial w}{\partial x}\right)^2\right]^2 \\
&\quad + \frac{1}{2}\left[\frac{1}{2}\left(\frac{\partial v}{\partial x}\right)^2 + \frac{1}{2}\left(\frac{\partial w}{\partial x}\right)^2\right]^3 - \frac{5}{8}\left[\frac{1}{2}\left(\frac{\partial v}{\partial x}\right)^2 + \frac{1}{2}\left(\frac{\partial w}{\partial x}\right)^2\right]^4 + ...,
\end{aligned}
\tag{11}
$$

where γ_{xz}, and γ_{yz} are transverse shear strains.

We represent the shape functions as follows: $N_1(x) = 1 - \frac{x}{a}$, $N_2(x) = \frac{x}{a}$, where a is the length of the finite element. The strain vector takes the form

$$
\boldsymbol{\varepsilon} = \begin{pmatrix} \varepsilon_x \\ \gamma_{xy} \\ \gamma_{xz} \end{pmatrix} = \mathbf{B}\mathbf{q}_e + \mathbf{N}_e(\mathbf{q}_e),
\tag{12}
$$

where

$$
\mathbf{B} = \begin{pmatrix}
-\dfrac{1}{a} & 0 & 0 & 0 & -\dfrac{y}{a} & -\dfrac{z}{a} & \dfrac{1}{a} & 0 & 0 & 0 & \dfrac{y}{a} & \dfrac{z}{a} \\[2mm]
0 & -\dfrac{1}{a} & 0 & \dfrac{z}{a} & \dfrac{1}{2} & 0 & 0 & \dfrac{1}{a} & 0 & -\dfrac{z}{a} & \dfrac{1}{2} & 0 \\[2mm]
0 & 0 & -\dfrac{1}{a} & -\dfrac{y}{a} & 0 & \dfrac{1}{2} & 0 & 0 & \dfrac{1}{a} & \dfrac{y}{a} & 0 & \dfrac{1}{2}
\end{pmatrix},
\tag{13}
$$

$$
\mathbf{N}_e = \begin{pmatrix}
\widehat{A} - \dfrac{1}{2}\widehat{A}^2 + \dfrac{1}{2}\widehat{A}^3 - \dfrac{5}{8}\widehat{A}^4 + ... \\
0 \\
0
\end{pmatrix},
\tag{14}
$$

$$
\widehat{A} = \frac{1}{2a^2}\left[(V_2 - V_1)^2 + (W_2 - W_1)^2\right],
$$

$$\mathbf{q}_e^T = \left(U_1\ V_1\ W_1\ \Theta_1\ B_{y,1}\ B_{z,1}\ U_2\ V_2\ W_2\ \Theta_2\ B_{y,2}\ B_{z,2} \right), \tag{15}$$

$\mathbf{B}$ is the strain matrix that determines the linear part of the longitudinal strains $\varepsilon_x^{\mathrm{lin}}$, $\mathbf{N}_e$ is the nonlinear operator that determines the nonlinear part of the longitudinal strains $\varepsilon_x^{\mathrm{nonlin}}$, $\mathbf{q}_e$ is the vector of nodal displacements, U_i, V_i, W_i are the values of the displacements u, v, w in node i, Θ_i is the torsion angle, $B_{y,i}, B_{z,i}$ are the values of the parameters of the rotation angles β_y, β_z at the nodes $i = 1, 2$ of the finite element, with e is denoting number. To ensure the absence of shear locking, the following interpolation is used: $\gamma_{xy}(x, z) = \frac{1}{2} \left[\gamma_{xy}(0, z) + \gamma_{xy}(a, z) \right]$, $z \leftrightarrow y$ in (13).

The strain vector variation, taking into account (12), is determined as follows:

$$\delta \boldsymbol{\varepsilon} = \mathbf{B} \cdot \delta \mathbf{q}_e + \frac{\partial \mathbf{N}_e\left(\mathbf{q}_e\right)}{\partial \mathbf{q}_e} \cdot \delta \mathbf{q}_e. \tag{16}$$

Let us denote

$$\mathbf{B}_{\mathrm{nonlin}} = \frac{\partial \mathbf{N}_e\left(\mathbf{q}_e\right)}{\partial \mathbf{q}_e} = \begin{pmatrix} 0 & \dfrac{\partial \Omega}{\partial V_1} & \dfrac{\partial \Omega}{\partial W_1} & 0 & 0 & 0 & 0 & \dfrac{\partial \Omega}{\partial V_2} & \dfrac{\partial \Omega}{\partial W_2} & 0 & 0 & 0 \\ 0 & 0 & 0 & 0 & 0 & 0 & 0 & 0 & 0 & 0 & 0 & 0 \\ 0 & 0 & 0 & 0 & 0 & 0 & 0 & 0 & 0 & 0 & 0 & 0 \end{pmatrix}, \tag{17}$$

$\Omega = \widehat{A} - \frac{1}{2}\widehat{A}^2 + \frac{1}{2}\widehat{A}^3 - \frac{5}{8}\widehat{A}^4 + \dots$. The derivatives of $\frac{\partial \Omega}{\partial V_1}, \frac{\partial \Omega}{\partial V_2}, \frac{\partial \Omega}{\partial W_1}, \frac{\partial \Omega}{\partial W_2}$ are easy to calculate, for example, $\frac{\partial \Omega}{\partial V_1} = -\left(1 - \widehat{A} + \frac{3}{2}\widehat{A}^2 - \frac{5}{2}\widehat{A}^3 + \dots\right) \cdot (V_2 - V_1)$. The proposed approach makes it quite easy to increase the number of terms in the Taylor expansion without changing the general algorithm. Here V_1, V_2, W_1, W_2 are the nodal values of the displacements v, w, corresponding to the achieved stress-strain state of the finite element. In the Newton–Raphson method used in this work, as in many step-by-step methods for solving the Cauchy problem containing nonlinear operators, we have

$$\boldsymbol{\varepsilon}\left(\mathbf{q}_e + \Delta \mathbf{q}_e\right) = \mathbf{B}\mathbf{q}_e + \mathbf{B}\Delta \mathbf{q}_e + \mathbf{N}_e\left(\mathbf{q}_e + \Delta \mathbf{q}_e\right)$$

$$= \mathbf{B}\mathbf{q}_e + \mathbf{B}\Delta \mathbf{q}_e + \mathbf{N}_e\left(\mathbf{q}_e\right) + \frac{\partial \mathbf{N}_e\left(\mathbf{q}_e\right)}{\partial \mathbf{q}_e}\Big|_{\mathbf{q}_e} \cdot \triangle \mathbf{q}_e, \tag{18}$$

where $\triangle \mathbf{q}_e$ is a small finite increment of the nodal displacement vector. The operator $\frac{\partial \mathbf{N}_e(\mathbf{q}_e)}{\partial \mathbf{q}_e}$ generating the matrix $\mathbf{B}_{\mathrm{nonlin}}$ is determined in the state corresponding to the vector $\mathbf{q}_e$, which is already known from the previous step of

solving the problem. In the physical sense, $\delta\left(\triangle\mathbf{q}_e\right) = \delta\mathbf{q}_e$, $\delta\left(\mathbf{B}\mathbf{q}_e\right) = 0$, because neither the $\mathbf{B}$ matrix nor the known $\mathbf{q}_e$ vector varies. For the same reason, $\delta\mathbf{N}_e\left(\mathbf{q}_e\right) = 0$. From Eq. (18), it yields:

$$\delta\boldsymbol{\varepsilon} = \left(\mathbf{B} + \mathbf{B}_{\mathrm{nonlin}}\right) \cdot \delta\mathbf{q}_e. \tag{19}$$

Repeating the above reasoning for the sth reinforcing rod, while taking into account the kinematic coupling conditions (6), we obtain:

$$\delta\boldsymbol{\varepsilon}_s = \left(\mathbf{B}_s + \mathbf{B}_{\mathrm{nonlin}}\right) \cdot \delta\mathbf{q}_e, \tag{20}$$

where $\mathbf{B}_s = \mathbf{B}\left(y_s, z_s\right)$ and the operator $\mathbf{B}_{\mathrm{nonlin}}$ is still defined by expression (17), since the displacements v and w do not depend on the coordinates y and z.

The first two terms of expression (3) represent the virtual work of the internal forces of the finite element, which, by the energy conservation law, is equal to the virtual work of the nodal reactions of the finite element $\delta\mathbf{q}_e^T \cdot \mathbf{r}_e^{\mathrm{int}}$. That is why:

$$\delta\mathbf{q}_e^T \left[\iiint\limits_V \left(\mathbf{B}^T + \mathbf{B}_{\mathrm{nonlin}}^T\right) \boldsymbol{\sigma} dV + \sum_s A_s \int\limits_0^a \left(\mathbf{B}_s^T + \mathbf{B}_{\mathrm{nonlin}}^T\right) \boldsymbol{\sigma}_s dx - \mathbf{r}_e^{\mathrm{int}} \right] = 0. \tag{21}$$

Here we have used expression (3) in vector form, so $\boldsymbol{\sigma}^T = \left(\sigma_x \quad \tau_{xy} \quad \tau_{xz}\right)$, $\boldsymbol{\sigma}_s^T = \left(\sigma_s \quad \tau_{sn} \quad \tau_{sz}\right)$. Due to the arbitrariness of variations, we obtain an expression for the internal forces of a finite element:

$$\mathbf{r}_e^{\mathrm{int}} = \iiint\limits_V \left(\mathbf{B}^T + \mathbf{B}_{\mathrm{nonlin}}^T\right) \boldsymbol{\sigma} dV + \sum_s \int\limits_0^a \left(\mathbf{B}_s^T + \mathbf{B}_{\mathrm{nonlin}}^T\right) \boldsymbol{\sigma}_s dx. \tag{22}$$

To determine the tangent stiffness matrix of a finite element, we represent Eq. (3) in a vector-incremental form:

$$\iiint\limits_V \delta\left(\boldsymbol{\varepsilon}^T + \triangle\boldsymbol{\varepsilon}^T\right) \left[\boldsymbol{\sigma}\left(\boldsymbol{\varepsilon}^T + \triangle\boldsymbol{\varepsilon}^T\right)\right] dV$$

$$+ \sum_s A_s \int\limits_0^a \delta\left(\boldsymbol{\varepsilon}_s^T + \triangle\boldsymbol{\varepsilon}_s^T\right) \cdot \left[\boldsymbol{\sigma}_s\left(\boldsymbol{\varepsilon}_s^T + \triangle\boldsymbol{\varepsilon}_s^T\right)\right] dx - \delta A_{\mathrm{ext}} = 0, \tag{23}$$

where $\triangle\boldsymbol{\varepsilon}$, $\triangle\boldsymbol{\varepsilon}_s$, are small finite increments of strain vectors. Taking into account that the components of the stress-strain state from the previous step are

known and do not vary, and according to the physical meaning of variations $\delta\left(\triangle\boldsymbol{\varepsilon}\right) = \delta\boldsymbol{\varepsilon}$ and $\delta\left(\triangle\boldsymbol{\varepsilon}_s\right) = \delta\boldsymbol{\varepsilon}_s$, we obtain:

$$\iiint\limits_{V} \delta\boldsymbol{\varepsilon}^T \cdot \left(\boldsymbol{\sigma} + \mathbf{C}_t \triangle \boldsymbol{\varepsilon}\right) dV + \sum_s A_s \int\limits_0^a \delta\boldsymbol{\varepsilon}_s^T \cdot \left(\boldsymbol{\sigma}_s + \mathbf{C}_t^s \triangle \boldsymbol{\varepsilon}_s\right) dx - \delta A_{\text{ext}} = 0, \quad (24)$$

because $\boldsymbol{\sigma}\left(\boldsymbol{\varepsilon} + \triangle\boldsymbol{\varepsilon}\right) = \boldsymbol{\sigma}\left(\boldsymbol{\varepsilon}\right) + \frac{\partial\boldsymbol{\sigma}}{\partial\boldsymbol{\varepsilon}}\big|_{\boldsymbol{\varepsilon}} \triangle\boldsymbol{\varepsilon} = \boldsymbol{\sigma}\left(\boldsymbol{\varepsilon}\right) + \mathbf{C}_t \triangle \boldsymbol{\varepsilon}$. Here, we use the expansion in a Taylor series with the retention of two terms. Likewise, $\boldsymbol{\sigma}_s\left(\boldsymbol{\varepsilon}_s + \triangle\boldsymbol{\varepsilon}_s\right) = \boldsymbol{\sigma}_s\left(\boldsymbol{\varepsilon}_s\right) + \mathbf{C}_t^s \triangle \boldsymbol{\varepsilon}_s$. Matrices $\mathbf{C}_t$ and $\mathbf{C}_t^s$ are determined according to the accepted material model. In the case of plastic flow theory, these are tangent consistent modular matrices [22]. Expression (24), taking into account the kinematic coupling conditions (6), is converted to the following form:

$$\delta\mathbf{q}_e^T \cdot \Bigg[\iiint\limits_{V} \left(\mathbf{B} + \mathbf{B}_{\text{nonlin}}\right)^T \mathbf{C}_t \left(\mathbf{B} + \mathbf{B}_{\text{nonlin}}\right) dV$$

$$+ \sum_s A_s \int\limits_0^a \left(\mathbf{B}_s + \mathbf{B}_{\text{nonlin}}\right)^T \mathbf{C}_t^s \left(\mathbf{B}_s + \mathbf{B}_{\text{nonlin}}\right) dx \Bigg] \cdot \triangle\mathbf{q}_e$$

$$= \delta A_{\text{ext}} - \left(\iiint\limits_{V} \delta\boldsymbol{\varepsilon}^T \cdot \boldsymbol{\sigma}\, dV + \sum_s A_s \int\limits_0^a \delta\boldsymbol{\varepsilon}_s \cdot \boldsymbol{\sigma}_s\, dx \right). \quad (25)$$

We represent the virtual work of external forces as $\delta A_{\text{ext}} = \delta\mathbf{q}_e^T \cdot \mathbf{f}_e^{\text{ext}}$, where $\mathbf{f}_e^{\text{ext}}$ is the vector of nodal values of forces due to a given load. According to Eqs. (19)–(21), the second term on the right-hand side of expression (25) is the virtual work of internal forces $\delta\mathbf{q}_e^T \cdot \mathbf{f}_e^{\text{int}}$. Therefore, (25) reduces to the following form:

$$\delta\mathbf{q}_e \cdot \left(\mathbf{K}_e^t \triangle \mathbf{q}_e - \mathbf{f}_e^{\text{ext}} + \mathbf{f}_e^{\text{int}}\right) = 0. \quad (26)$$

By the arbitrariness of variations, the expression inside the parentheses is identically equal to zero. This expression represents one step of the Newton–Raphson method, which we obtained based on the principle of virtual work. The tangent stiffness matrix $\mathbf{K}_e^t$ of the finite element e is given by the expression in square brackets of Eq. (25).

2.3. Shell finite elements

Quadrilateral and triangular isoparametric flat shell finite elements in a geometrically linear formulation are presented in [18, 23, 24]. We will omit the

resolving relations due to their cumbersome nature, and refer readers interested in details to the mentioned sources, believing that the addition of geometrically nonlinear relations for the quadratic approximation model is well presented in many literature sources.

To take into account a geometrical nonlinearity, we use the classical approach based on total Lagrangian formulation. The Cauchy–Green strain tensor with quadratic approximation of nonlinear part is applied. This approach allows to describe the initial post-buckling behavior of thin-walled plates, as well as to consider the interaction of membrane and bending components of internal forces in the middle surface.

The Gauss–Legendre method is applied for numerical integration in the finite element area, and the trapezoidal method is used in the thickness direction. So, the finite element is divided into layers across thickness, and the components of the stress and strain tensors are determined at the Gaussian integration points in each layer. Internal forces such as longitudinal, transverse, shear forces, and bending moments are determined by integrating the corresponding components of the stress tensor over the thickness of the finite element. These force factors are not directly involved in the solution procedure and they are calculated at the points of result storage only for the convenience of the user. An integration scheme of 2×2 is used for each layer of the quadrilateral finite element, and 1×1 for each layer of the triangular one.

Reinforcing rods are represented as reinforcing layers, with each layer consisting of identical reinforcing rods aligned in the same direction. So, the reinforcing rods are smeared in the plane of the finite element, but the discreteness of their placement along the thickness is preserved. In actual real finite element meshes, each reinforcing layer contains several reinforcing rods, which justifies their smearing in the plane of the layer. Kinematic coupling conditions are used to ensure the compatibility of deformations between the concrete and the reinforcements for the case where no slips are assumed.

Mixed Interpolation of Tensorial Components (MITC) technique [25] as well as Discrete Shear Gap (DSG) method [26] are applied to avoid the transversal shear locking effect for quadrilateral and triangular finite elements, respectively.

To obtain the tangent stiffness matrix and the vector of internal forces, the same variational approach is applied as for the spatial frame finite element.

2.4. Numerical solution procedure

The proposed finite elements require a lot of computational work; so, we apply multi-threaded parallelization to reduce the duration of calculations. The use of dense matrix multiplication and matrix-vector multiplication procedures implemented in the Intel Math Kernel Library [27] which include vectorization

and efficient use of processor pipelines also improves performance. The equations of motion of the finite element model are presented as follows:

$$\begin{cases} \mathbf{M\ddot{u} + C\dot{u} + f^{\text{int}}}\left(\mathbf{u, \dot{u}}\right) = \mathbf{f^{\text{ext}}}, \\ \mathbf{u}\left(0\right) = \mathbf{u}_0, \qquad \mathbf{\dot{u}}\left(0\right) = 0, \end{cases} \tag{27}$$

where $\mathbf{M}$ and $\mathbf{C}$ are the mass and dissipation matrices, respectively, $\mathbf{f}^{\text{int}}$ is a non-linear operator returning the vector of internal forces, $\mathbf{f}^{\text{ext}}$ is a vector of external forces caused by dead and live loads, $\mathbf{u}$ is a displacement vector, and $\mathbf{u}_0$ is an initial displacement vector obtained from the solution of the static nonlinear problem:

$$\mathbf{f}^{\text{int}}\left(\mathbf{u}_0\right) = \mathbf{f}^{\text{ext}}. \tag{28}$$

Thus, the nonlinear static problem (28) is first solved and the displacement vector $\mathbf{u}_0$ as well as the stress-strain state of all nonlinear finite elements are determined. These results are used as initial conditions for solving the Cauchy problem (27). The initiation of motion is produced by the instantaneous removal of the designated finite elements at given times according to the selected scenario, which leads to a violation of the equilibrium of the structure achieved when solving problem (28) by the Newton–Raphson method.

Calculation models of multi-story buildings containing plate and shell finite elements have high natural frequencies; therefore, the application of conditionally stable explicit methods for numerical integration of the Cauchy problem (27) requires the use of very small time steps, and, accordingly, much more processor time than implicit methods require. In addition, in explicit methods, the dissipation matrix $\mathbf{C}$ must be diagonal, which leads to an underestimation of damping in the higher modes and can significantly distort the dynamic behavior of building structures.

On the other hand, in cases where differential equations have discontinuous parameters, explicit methods have higher computational stability than implicit ones. The discontinuity of the parameters in the differential equations arises due to the destruction of concrete in the tension and compression zones, as well as the ruptures of reinforcing rods.

So, the implicit predictor-corrector method [18, 28], is applied to solve the Cauchy problem (27), in which the Newton–Raphson method is used at each step of the corrector iterations to achieve equilibrium of the system with a given accuracy. For the effective suppression of high-frequency oscillations, which often lead to deterioration in the convergence of implicit numerical methods, the $\alpha - HHT$ method is used [29]. At the predictor stage, we have:

$$\begin{cases} \widehat{\mathbf{u}}_{k+1-\widehat{\alpha}} = \left(1 - \widehat{\alpha}\right)\widehat{\mathbf{u}}_{k+1} - \widehat{\alpha}\widehat{\mathbf{u}}_k, \\ \widehat{\mathbf{v}}_{k+1-\widehat{\alpha}} = \left(1 - \widehat{\alpha}\right)\widehat{\mathbf{v}}_{k+1} - \widehat{\alpha}\widehat{\mathbf{v}}_k, \end{cases} \tag{29}$$

where $\widehat{\alpha} \in (-0.3333, 0]$, k is the time step number, and $\mathbf{v} = \dot{\mathbf{u}}$ is the nodal velocity vector,

$$\begin{cases} \widehat{\mathbf{u}}_{k+1} = \mathbf{u}_k + \triangle t \mathbf{v}_k + \dfrac{\triangle t^2}{4}\mathbf{a}_k, \\[2mm] \widehat{\mathbf{v}}_{k+1} = \mathbf{v}_k + \dfrac{\triangle t}{2}\mathbf{a}_k, \qquad \widehat{\mathbf{a}}_{k+1} = 0, \end{cases} \qquad (30)$$

where $\widehat{\mathbf{u}}_{k+1}$, $\widehat{\mathbf{v}}_{k+1}$, $\widehat{\mathbf{a}}_{k+1}$ are the predictions of displacement, velocity and acceleration vectors at the time step $k+1$, $\triangle t$ is the time step value, and $\mathbf{a} = \ddot{\mathbf{u}}$.

The corrector algorithm (Algorithm 1) is presented to show exactly where the instantaneous removal of finite elements is performed, as well as to visualize the stages to which multithreaded parallelization is applied.

Algorithm 1. Corrector stage.

1:   $i = 0$;

2:   **while** $i < iter\_max$ **do**

3:      $\mathbf{r} = \mathbf{f}^{\text{ext}}_{k+1-\widehat{\alpha}} - \mathbf{f}^{\text{int}}_{k+1-\widehat{\alpha}} - \mathbf{M}\mathbf{a}^i_{k+1} - \mathbf{C}\mathbf{v}^i_{k+1-\widehat{\alpha}}$

4:      **if** $\|\mathbf{r}\|_2 < tol$ **then**

5:         *break;*

6:      **end if**

7:      $\mathbf{K}^t_{\text{dyn}}\left(\mathbf{u}^i_{k+1-\widehat{\alpha}}\right) = \dfrac{1}{\beta \triangle t^2}\mathbf{M} + (1+\widehat{\alpha})\dfrac{\gamma}{\beta \triangle t}\mathbf{C} + (1+\widehat{\alpha})\mathbf{K}^t\left(\mathbf{u}^i_{k+1-\widehat{\alpha}}\right)$

8:      $\mathbf{K}^t_{\text{dyn}} = \mathbf{LSL}^T$

9:      $\mathbf{LSL}^T \cdot \triangle \mathbf{u} = \mathbf{r} \quad \rightarrow \quad \triangle \mathbf{u}$

10:     $\mathbf{u}^{i+1}_{k+1} = \mathbf{u}^i_{k+1} + \triangle \mathbf{u}$

11:     $\mathbf{u}^{i+1}_{k+1-\widehat{\alpha}} = (1+\widehat{\alpha})\mathbf{u}^{i+1}_{k+1} - \widehat{\alpha}\mathbf{u}_k$

12:     $\mathbf{a}^{i+1}_{k+1} = \dfrac{1}{\beta \triangle t^2}\left(\mathbf{u}^{i+1}_{k+1} - \widehat{\mathbf{u}}_{k+1}\right)$

13:     $\mathbf{v}^{i+1}_{k+1} = \widehat{\mathbf{v}}_{k+1} + \gamma \triangle t \, \mathbf{a}^{i+1}_{k+1}$

14:     $\mathbf{v}^{i+1}_{k+1-\widehat{\alpha}} = (1+\widehat{\alpha})\mathbf{v}^{i+1}_{k+1} - \widehat{\alpha}\mathbf{v}_k$

15:     $i++$

16: **end while**

Here $\beta = \dfrac{(1+\widehat{\alpha})^2}{4}$, $\gamma = \frac{1}{2} - \widehat{\alpha}$, $iter\_max$ is a maximum number of iterations at the corrector stage. The corrector algorithm is entered with the vectors $\mathbf{u}^0_{k+1} = \widehat{\mathbf{u}}_{k+1}$, $\mathbf{v}^0_{k+1} = \widehat{\mathbf{v}}_{k+1}$, $\mathbf{a}^0_{k+1} = \widehat{\mathbf{a}}_{k+1} = 0$ (30), which were obtained at the predictor

stage. When determining the residual vector $\mathbf{r}$ (step 3), the most time-consuming procedure is to calculate the internal forces vector:

$$\mathbf{f}_{k+1-\widehat{\alpha}}^{\text{int}} = \mathbf{N}\left(\mathbf{u}_{k+1-\widehat{\alpha}}^i, \mathbf{v}_{k+1-\widehat{\alpha}}^i\right) + \mathbf{K}_{\text{lin}}\mathbf{u}_{k+1-\widehat{\alpha}}^i, \tag{31}$$

where $\mathbf{N}(...)$ is a nonlinear operator returning the internal forces generated by nonlinear finite elements, and $\mathbf{K}_{\text{lin}}$ is a stiffness matrix composed only of linear finite elements. Real computational models contain, as a rule, both linear and nonlinear finite elements. The contribution of linear finite elements to the internal forces of the system on multi-core computers is usually faster to determine by multiplying the sparse matrix $\mathbf{K}_{\text{lin}}$, which is assembled and stored in a compressed format, with the vector of nodal displacements.

Multithreaded parallelization covers all stages of the implicit method for solving the Cauchy problem (27). Original in-home algorithms for parallelizing the assembly of the tangential stiffness matrix (Algorithm 3) and calculating the internal forces (Algorithm 2) are presented. Parallel algorithms of symmetric sparse matrix factorization and forward and backward substitutions are presented in [30] and [31]. The parallelization of the remaining parts of the method is reduced to the parallelization for loops in (29), (30) and steps 10–14 of Algorithm 1.

The nonlinear operator $\mathbf{N}(...)$ is represented by Algorithm 2. At step 1, the vector of internal forces $\mathbf{f}_{\text{nonlin}}^{\text{int}}$, formed by the contribution of only nonlinear finite elements, is set to zero, as well as the auxiliary vectors $\mathbf{rr}_{ip} \leftarrow 0, ip \in [0, np-1]$. Here and below, ip is the thread number, and np is the number of threads.

Algorithm 2. Internal force vector evaluation. Nonlinear operator.

1: $\mathbf{f}_{\text{nonlin}}^{\text{int}} \leftarrow 0; \quad \mathbf{rr}_{ip} \leftarrow 0, \ ip \in [0, np-1]$

2: **for parallel** $e \in NonlinFE$ **do**

3:     **if** $e \notin DestructedFE$ **then**

4:         $\mathbf{u}_e \leftarrow \widehat{\mathbf{u}}_{k+1-\widehat{\alpha}}^i$

5:         $\mathbf{u}_e^{\text{loc}} = \mathbf{T}_e \mathbf{u}_e$

6:         $\mathbf{r}_e^{\text{int}} = GetNonlinInternForces(\mathbf{u}_e^{\text{loc}})$

7:         $\mathbf{rr}_{ip} \leftarrow \mathbf{T}_e^T \mathbf{r}_e^{\text{int}}$

8:     **end if**

9: **end for**

10: $\mathbf{f}_{\text{nonlin}}^{\text{int}} += \sum_{ip=0}^{np-1} \mathbf{rr}_{ip}$

In a loop **for parallel** (steps 2–9), on each thread $ip \in [0, np-1]$, the vectors $\mathbf{rr}_{ip}$ (steps 4–7) are calculated, and only the contribution of non-removed non-

linear finite elements ($e \notin DestructedFE$) is taken into account, since this loop covers only nonlinear finite elements ($e \in NonlinFE$). Here $NonlinFE$ is the set of nonlinear finite elements and $DestructedFE$ is the set of removed finite elements. The components of the nodal displacements vector corresponding to the degrees of freedom of the finite element e are selected (step 4). Then, the vector of nodal displacements as well as the vector of internal forces $\mathbf{r}_e^{\mathrm{int}}$ of this finite element in the local coordinate system are determined (steps 4 and 5) – the function $GetNonlinInternForces(\mathbf{u}_e^{\mathrm{loc}})$ evaluates expressions (22) for the spatial frame finite element or similar expressions for the shell ones (step 6). Here $\mathbf{T}_e$ is the transformation matrix associated with the transition from the global coordinate system to the local one and vice versa. Each thread ip adds the components of the vector of internal forces of the finite element e in the global coordinate system to its local vector $\mathbf{rr}_{ip}, ip \in [0, np-1]$, (step 7), whose dimension is equal to the number of equations of the entire system Neq. Upon completion of the parallel region, the vectors of internal forces $\mathbf{rr}_{ip}$ are gathered into a vector $\mathbf{f}_{\mathrm{nonlin}}^{\mathrm{int}}$ (step 10), and this gathering procedure is also parallelized. The vectors $\mathbf{f}_{\mathrm{nonlin}}^{\mathrm{int}}$, $\mathbf{rr}_{ip}$ and $\mathbf{u}_{k+1-\widehat{\alpha}}^i$ have the dimension Neq, and the dimension of the vectors $\mathbf{u}_e$, $\mathbf{u}_e^{\mathrm{loc}}$ and $\mathbf{r}_e^{\mathrm{int}}$ is equal to the number of degrees of freedom of the finite element e. Writing data by each thread to its vector $\mathbf{rr}_{ip}$, $ip \in [0, np-1]$, avoids thread competition in the parallel region. The multiplication of the sparse matrix $\mathbf{K}_{\mathrm{lin}}$ by a vector of nodal displacements $\mathbf{u}_{k+1-\widehat{\alpha}}^i$ is performed on a single thread, as it usually takes much less time than Algorithm 2.

All deleted elements must belong to the set $DestructedFE$, and the $\mathbf{K}_{\mathrm{lin}}$ matrix does not depend on time. The vectors $\mathbf{u}_e$, $\mathbf{u}_e^{\mathrm{loc}}$, $\mathbf{r}_e^{\mathrm{int}}$, and the transformation matrix $\mathbf{T}_e$ must be placed in the local memory of each thread to avoid thread competition.

Algorithm 3 represents a multi-threaded assembly of a sparse matrix $\mathbf{K}^t\big(\mathbf{u}_{k+1-\widehat{\alpha}}^i\big)$. At the initialization stage, an adjacency graph for the finite elements $AdjGraphFE$ is created. Additionally, the $task\_par$ queue, which includes the sequential numbers of the finite elements $1, 2, ..., Nele$, the $elem\_status$ array and the counter of assembled elements, referred to as $count$ (step 1) are all reset to zero. Here, $Nele$ is the number of finite elements in the design model. If $elem\_status[ele] = 0$, then the finite element ele participates in the assembly, but all its neighbors $ele\_nab \in AdjGraphFE(ele)$ do not participate in the assembly at this step. Such a strategy prevents the situation where in the parallel region several finite elements contribute to the same degrees of freedom at once. In the **parallel region** (steps 2–21), **while** loops, the number of which is equal to the number of threads, perform the assembly of the sparse matrix. In the critical section **lock 1** – **unlock 1**, the nearest finite element $ele \leftarrow task\_par$ is selected from the $task\_par$ queue and removed from the queue ($task\_par/ele$ – step 6). If $elem\_status[ele] = 0$ and ele does not belong to the set of removed

Algorithm 3. Multithreaded assembling of the sparse matrix $\mathbf{K}^t\left(\mathbf{u}^i_{k+1-\widehat{\alpha}}.\right)$.

1: Initialization: prepare $AdjGraphFE$, $task\_par$, $elem\_status \leftarrow 0$ and $count = 0$

2: **parallel region**

3: **while** $count < Nele$ **do**

4:     $flag\_continue = 0$;

5:     **lock 1**

6:         $ele \leftarrow task\_par\,(task\_par/ele)$

7:     **if** $!elem\_status[ele]$ **then**

8:         $\forall ele\_nab \in AdjGraphFE(ele)\colon elem\_status[ele\_nab] + +$;

9:     **else**

10:         $task\_par \leftarrow ele$; $flag\_continue = 1$;

11:     **end if**

12:     **unlock 1**

13:     **if** $flag\_continue$ **then** $continue$;

14:     **if** $ele \in DestructedFE$ **then** $goto$ 16;

15:     $\mathbf{K}^t\left(\mathbf{u}^i_{k+1-\widehat{\alpha}}\right) \leftarrow AddKe\left(ele, \mathbf{u}^i_{k+1-\widehat{\alpha}}\right)$

16:     **lock 2**

17:         $\forall ele\_nab \in AdjGraphFE(ele)\colon elem\_status[ele\_nab] - -$;

18:         $elem\_status[ele] = -1$; $count + +$;

19:     **unlock 2**

20: **end while**

21: **end of parallel region**

finite elements (steps 7 and 14), then the stiffness matrix $\mathbf{K}^t_e$ of the finite element ele will be calculated and added to the sparse matrix structure – procedure $AddKe(ele, \mathbf{u}^i_{k+1-\widehat{\alpha}})$ (step 15). In this case, for all neighbors of the finite element ele, the corresponding elements of the $elem\_status$ array are increased by one. This ensures that none of the **while** loops executed on other threads will allow the finite elements $ele\_nab \in AdjGraphFE(ele)$ – the neighbors of the finite element ele selected for assembly – to participate in the assembly until their status becomes zero again. If $elem\_status[ele] > 0$, then the finite element ele selected from the $task\_par$ queue is added to its end (step 10), and at later steps, an attempt will be made to start this finite element for assembly again. The **while** loop then proceeds to the next iteration (step 13).

If the finite element *ele* belongs to the set of removed elements, its stiffness matrix does not take part in the assembly (step 14), and the finite element itself is marked as already added (steps 16–19). As soon as the stiffness matrix of the finite element *ele* is added to the sparse matrix structure, in the **lock 2 – unlock 2** critical section, the status of the element *ele* is set to -1, the statuses of its neighbors *ele_nab* are decremented, and the counter of assembled finite elements is incremented (steps 16–19). As soon as all finite elements are assembled (*count == Nele*), the **while** loops will be interrupted and exit from the **parallel region** will follow.

The presented parallel assembly algorithm differs from the one published earlier in [30], Algorithm 4, in that the latter does not take into account the removal of destroyed finite elements from assembling. For large-dimensional problems, the mass matrix is usually diagonal, making all calculations related to it extremely fast (steps 3 and 7, Algorithm 1). When removing the destroyed elements, we do not change the inertial properties of the system, since usually, during a partial collapse, the debris is collected on the floor slabs – the rigidity of the system decreases, and the mass remains unchanged. The system of linearized algebraic equations is solved by the supernodal multithreaded PARFES solver [30], while the procedures for forward and backward substitutions are described in [31]. At the beginning of each integration step of the Cauchy problem (27), the set of removed elements $DestructedFE : ele \rightarrow DestructedFE \mid t \geq t_{ele}^{\mathrm{destr}}$ is determined. Here t, t_{ele}^{destr} are the current time moment and the time of removal of the finite element *ele*, respectively, and the symbol "$\rightarrow$" means the addition of the element *ele* to the *DestructedFE* set.

Some scenarios for removing finite elements from the initial design model can lead to the appearance of "hanging" nodes, that is, nodes that do not belong to any finite elements. As a result, the geometric instability of the design model appears. To overcome this problem, we use a regularization of the tangent stiffness matrix:

$$\forall eqn \in IsolEqn : \mathbf{K}_{eqn,eqn}^{t} + = \frac{1}{2} \max_{1 \leq i \leq Neq} \{\mathbf{M}_{i,i}\} \cdot \omega_{\max}^{2}, \qquad (32)$$

where $IsolEqns$ is the set of equations corresponding to the degrees of freedom of the "hanging" nodes, eqn is the current number of the equation, $\mathbf{K}_{eqn,eqn}^{t}$ is the diagonal element of the tangent stiffness matrix, $\max_{1 \leq i \leq Neq} \{\mathbf{M}_{i,i}\}$ is the largest diagonal element of the mass matrix, $\omega_{\max}^{2}$ is the highest natural frequency of the design model determined by the method of matrix iterations, and the factor $\frac{1}{2}$ divides half the interval from zero to $\omega_{\max}^{2}$. Since the expression on the right-hand side of Eq. (32) serves as a regularizing term, there is no need to determine the highest natural frequency with great accuracy. Therefore, even

for large computational models, it is determined in just a few seconds. Adding a regularizing parameter to the equations $eqn \in IsolEqn$ also requires a correction in the corresponding elements of the internal forces vector:

$$\forall eqn \in IsolEqn : \mathbf{f}_{\text{int},eqn}^{\text{nonlin}} + = \frac{1}{2} \max_{1 \le i \le Neq} \{\mathbf{M}_{i,i}\} \cdot \omega_{\max}^2 \cdot \mathbf{u}_{k+1-\widehat{\alpha},eqn}^i, \quad (33)$$

because otherwise, the iterations of the corrector (Algorithm 1) may diverge. This method of determining the regularizing parameter works for both the implicit method used in the proposed approach and the explicit one, and since in the latter case the tangent stiffness matrix of the entire system does not exist, the regularization parameter is determined based on the inertial characteristics of the system, and not the stiffness characteristics.

3. Substantiation of the reliability and effectiveness of the proposed approach

The justification for the reliability of the proposed approach is based on a comparison of the results of a numerical solution with the results of well-established experiments, exact analytical solutions in those rare cases when they exist, and reliable numerical solutions from other authors. Results of these comparisons for the problems of static loading of rectangular reinforced concrete plates are presented in [18, 23, 32], for the problems of transverse bending of reinforced concrete beams – in [18, 33], and results from tests of compressed reinforced concrete columns under cyclic loading – in [24]. The results presented in [23, 24, 32, 33] are available online; so, in this paper, we present comparison results that have not been published before.

Example 1 demonstrates the effectiveness of the proposed method for modeling the initial post-buckling behavior of a compressed elastic rod. In Example 2, taking into account both physical and geometrical nonlinearity, the deformation of a reinforced concrete column subjected to an eccentrically applied compressive load is considered. Example 3 confirms the feasibility of the proposed approach for modeling the progressive collapse of a two-story building consisting of columns and floor slabs stiffened by contour ribs. The validation and verification of the quadrilateral shell element as well as the spatial frame are also addressed.

The computational efficiency of the proposed approach is further demonstrated using speed-up curves with increasing the number of threads, both for the entire procedure of numerical integration of the Cauchy problem and for its principal stages – Example 4.

3.1. Example 1

The longitudinal-transverse bending of a simply supported beam under the action of an axial compressive force and a small transverse load that initi-

ates lateral buckling is considered (Fig. 3). Young's modulus is assumed to be $E = 210\,000$ MPa. The beam is divided into 40 finite elements. The problem is solved in an elastic formulation. The value of the critical force for the centrally compressed beam is $N_{cr} = \frac{\pi^2 EI}{a^2} = 107.776$ MN. Here, I and a are the moment of inertia of the cross-section and the length of the beam, respectively. This example is taken from [34] (Sec. 3 for source data).
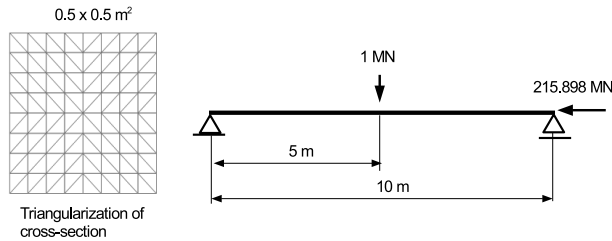

FIG. 3. Lateral buckling of the beam under the action of longitudinal compressed force and small transverse load.

Figure 4 shows the behavior of the numerical solution when retaining between two and sixteen terms in the Taylor series expansion (curves h-2, h-4, ..., h-16) – expression (14). The "exact analytical solution" curve corresponds to the post-buckling behavior of a Bernoulli beam under axial compression, taking into account the exact expression for the change in curvature, and is taken from [35]. The horizontal straight line labeled "critical force" separates the regions of post-buckling and pre-buckling deformation on the chart.
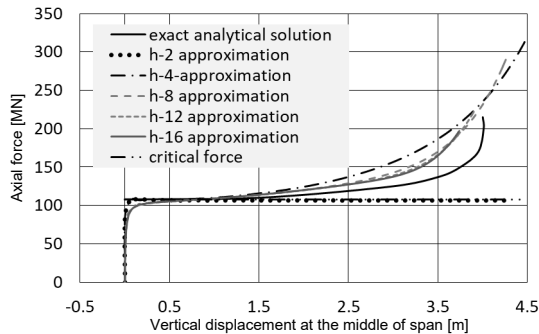
FIG. 4. Post-buckling behavior of the numerical solution while holding a different number of series terms in the Taylor expansion.

Usually, two terms in the Taylor series expansion are retained (curve "h-2") when the buckling of a rod is considered. However, this approach does not allow exceeding the critical load, so it is unsuitable for modeling post-buckling behavior. Approximations h-4–h-16 bring the numerical solution closer to the exact analytical one and make it possible to fairly accurately describe the initial

post-buckling behavior of the rod during buckling. A more accurate approxima-
tion can be obtained using the updated Lagrangian formulation approach – the
"update coord" curve in Fig. 5. The proposed in the given article method is much
easier to implement than the updated Lagrangian formulation. In addition, it
usually requires fewer iterations, fewer load steps, and less often demonstrates
a lack of convergence. Taking into account the fact that in structural mechanics
problems, we are unlikely to have to simulate the curvature of a compressed elas-
tic rod to the extent of forming closed ring, for solving further problems we will
use the proposed approach based on total Lagrangian formulation and keeping
high-order terms in the Taylor series expansion.
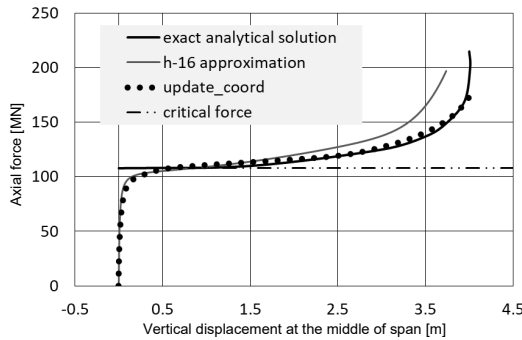
FIG. 5. Post-buckling behavior of the numerical solution for different approaches.

3.2. Example 2

The buckling of a compressed column with eccentricity is considered (Fig. 6a).
The problem is solved using an elasto-plastic formulation with geometric non-
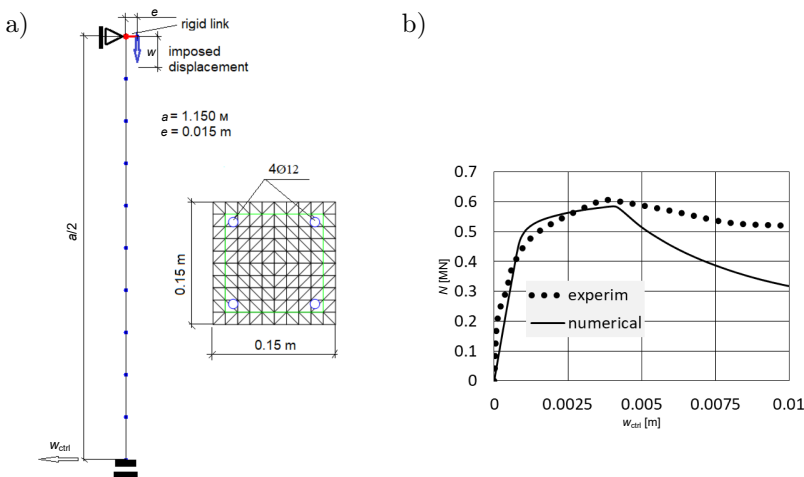
FIG. 6. a) Design model, b) longitudinal force in the bottom finite element
versus control displacement.

linearity taken into account. The physical and mechanical characteristics of the concrete and reinforcement are as follows: $E = 30000$ MPa, $\sigma_t = 2.0$ MPa, $\sigma_c = 30$ MPa, $\nu = 0.2$, $E_s = 200\,000$ MPa, $\sigma_y = 560$ MPa.

Here, E_s and σ_y are the Young's modulus and yield strength for steel. This example is taken from [36]. In the design model, half of the column is considered, with the lower support modeling the symmetry conditions. The eccentricity e is created by a rigid body, at the free end of which the vertical displacement w is given. Dividing the column into spatial frame finite elements, presented in Subsec. 2.2, is shown in Fig. 6a. Figure 6b presents a comparison of the proposed numerical solution ("numerical" curve) with the experimental results ("experim" curve) taken from [36]. The outlines of these curves are similar up to the limit point with a difference in bearing capacity of 3% in the vicinity of the limit point. This indicates the effectiveness of the proposed spatial frame finite element.

3.3. Example 3

Figure 7 shows the design model of the experimental sample, the tests of which are presented in [37]. The thickness of the floor slabs is 20 cm.
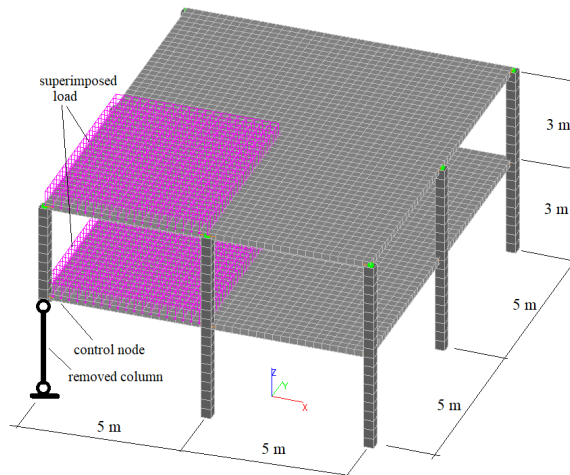
FIG. 7. Design model of the experimental sample.

Since, in thin plates, the application of concentrated forces, which are normal to the middle surface, turns out to be a logarithmic singularity in the bending moments [38], the refinement of mesh leads to divergence in the internal forces. Therefore, we establish rigid links [39] on the nodes adjacent to the node of the intersection of the column axis with the middle surface of the floor slab. These rigid bodies are not shown in order not to complicate the drawing of Fig. 7.

The floor slabs are reinforced along the contour with stiffening ribs, modeled as spatial frame finite elements with a cross-section of 20×30 cm (Fig. 8). Sections of the columns are also shown in Fig. 8, with the central column having stronger reinforcement. The upper and lower reinforcement of the floor slabs consists of rods 12 mm in diameter spaced apart 200 mm in two directions. In addition, the upper reinforcement above the columns is increased as described in [37].
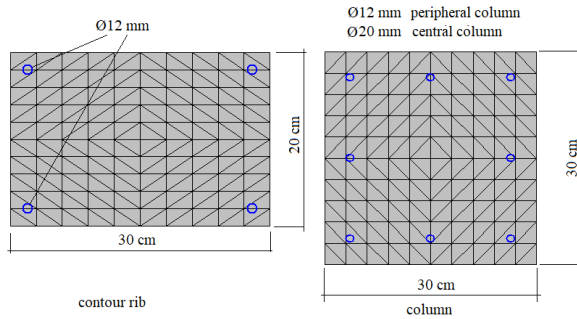

FIG. 8. Meshing and cross-sections of the spatial frame finite elements.

The following physical and mechanical characteristics of concrete and steel are accepted: $E = 30\,000$ MPa, $\sigma_t = 2.44$ MPa, $\sigma_c = 30$ MPa, $\nu = 0.2$, $\rho = 2400$ kg/m^3, $E_s = 200\,000$ MPa, $\sigma_y = 500$ MPa. Here, ρ is the density of concrete. In addition, we take a maximum deviation of yield surface from a circular shape: $\overline{\alpha} = 0.532$ (expression (1), Subsec. 2.1) and $\varepsilon_u = 0.004935$ – Fig. 1.

The dead load as well as the uniformly distributed superimposed load is applied in the bay comprising the removed column (Fig. 7). The removed corner column is modeled as an elastic steel rod with an I-section (see [37]). When the column is removed, the trigger device operates with a delay of about 0.1 s. To simulate this phenomenon, at the moment of removal of the column, a reaction is applied, which then decreases to zero according to a linear law. The elasto-plastic behavior of concrete and steel, as well as geometric nonlinearity, is taken into account.

Figure 9 shows the vertical displacement of the controlled node located near the removed column. Curve "numerical: delay 0.1 s" corresponds to the delay in a trigger device of considered test, curve "numerical: delay = 0 s" corresponds to the immediate removal of a column, and curve "numerical: delay = 0.995 s" presents a very slow removal of the column, when dynamical effects are negligibly small. The last curve demonstrates the fact that ignoring dynamic effects leads to a significant distortion of the numerical prediction. Thus, the behavior of the structure depends on how quickly the destroyed elements are removed. This is consistent with the results given in [9]. When solving real-life problems, information about the velocity of removal of elements from the calculation model is usually unknown. In addition, both in the considered example and in [9], in-
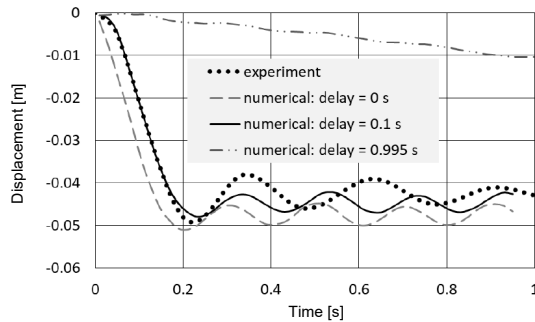
Fig. 9. Vertical displacements in the control node.

stantaneous removal corresponds to the largest displacements of the calculation model nodes, therefore, in all subsequent examples, we will consider instantaneous removal believing that it is the most dangerous.

We obtained a maximum deflection value close to the experimental results (curve "numerical: delay = 0.1 s"). However, the period of free vibrations after removing the corner column in the proposed approach is slightly higher than in the experiment. Taking into account the fact that when performing progressive failure analysis, the main question is whether progressive destruction will occur or not, we conclude that the proposed method leads to acceptable results since both the numerical solution and the experimental results demonstrate the oscillatory nature of the behavior of structural elements with similar maximum displacements after the initiating impact.

3.4. Example 4

Figure 10 shows a design model of a typical multi-story building containing 1027082 equations, with both physical and geometric nonlinearity taken into account for all finite elements. The solution of the Cauchy problem (27) for nonlinear computational models of large dimensions is a very time-consuming procedure. Therefore, in this paper, to speed up the solution of such a problem, we primarily use multithreaded parallelization.

Table 1 shows the time taken for solving the principal stages as well as the time for the complete solution of the Cauchy problem (27) depending on the number of threads. Here, Assembling refers to the assembly of the dynamic tangent stiffness matrix (step 7, Algorithm 1), Residual vector – the calculation of the residual vector (step 3, Algorithm 1), Factorization – (step 8, Algorithm 1), Resol. – forward and backward substitutions (step 9, Algorithm 1), Rest – other stages of solving the Cauchy problem, parallelization of which is reduced to the parallelization of the corresponding **for** loops, and Total – the total computation time.
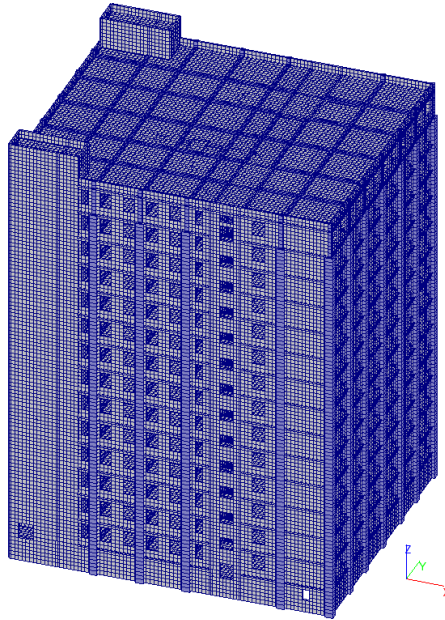
Fig. 10. Design model of a multi-story building (1 027 082 equations).

Table 1. Duration of the principle stages ofthe Cauchy problem [s].

# threads	Assembling	Residual vector	Factorization	Resol.	Rest	Total
1	7164	2006	8642	207	248	18267
2	3736	1042	4760	134	179	9851
4	1813	520	2241	96	133	4803
6	1298	362	1706	99	131	3596
8	1019	283	1474	99	134	3009
10	851	238	1146	98	134	2467
12	729	204	1133	98	134	2299

A desktop computer with a 12-core Intel Core$^{\text{TM}}$ i9-9920X CPU 3.50 GHz processor, 12 physical cores, and 24 logical processors, is used. The amount of RAM is 128 GB with four memory channels allows us to keep the entire problem in the core memory. The considered problem requires 23.7 GB RAM. This processor supports SIMD instructions AVX512F and FMA, which ensures high performance during the factorization stage. Figure 11 shows the dependence of speed up $S_p = T_1/T_p$ on the number of threads, where T_1 is the time to solve the problem using a single thread, T_p is the time to solve the problem with p threads. The Assembling and Residual vector stages turned out to be the most accelerated, which confirms the effectiveness of Algorithms 2 and 3. Conversely, the

Resol. stage is the least accelerated since the Cauchy problem is solved with a single right-hand side (step 8, Algorithm 1).
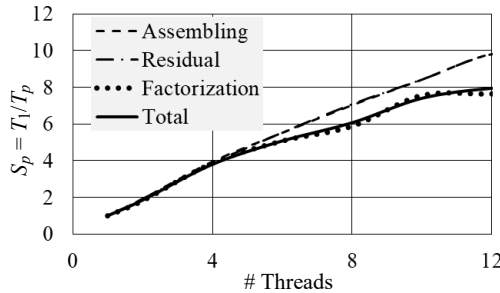

Fig. 11. Speedup of the principal stages of the Cauchy problem.

The proposed approach has a stable acceleration with an increase in the number of threads up to the number of physical processor cores and makes it possible to achieve an 8-fold reduction in analysis time when using 12 threads. We emphasize that this result was obtained for solving the entire Cauchy problem, and not for individual classical linear algebra algorithms.

Thus, a comparison of the numerical results obtained by the proposed approach with the experimental results, as well as with the numerical and analytical solutions of other authors, shows that the proposed method demonstrates results acceptable for engineering practice, and, in addition, makes this type of analysis more accessible in terms of time spent on multi-core computers of the Symmetric Multiprocessing (SMP) architecture.

4. Numerical results

Unlike the vast majority of articles and scientific reports, in which the initiating action is the instantaneous removal of one or another column, in this section we will consider the design models of multi-story buildings in which elements of the staircase-elevator block (Fig. 12) are removed. These elements are the most important load-bearing elements in the structures of modern multi-story buildings. Another important point that needs to draw attention is that while most works, one way or another, stimulate the behavior of the structure after the sudden removal of the specified structural elements, there are no proposals on how to make sure that this does not lead to the occurrence of a progressive collapse. One of the approaches aimed at improving the reliability of the structure is the installation of reinforcing elements on the upper floor of the building (creation of an outrigger floor), which must hang a section of the building, from under which the columns of the lower floor (or other types of load-bearing elements) were suddenly removed, and to redistribute forces in the structural elements to
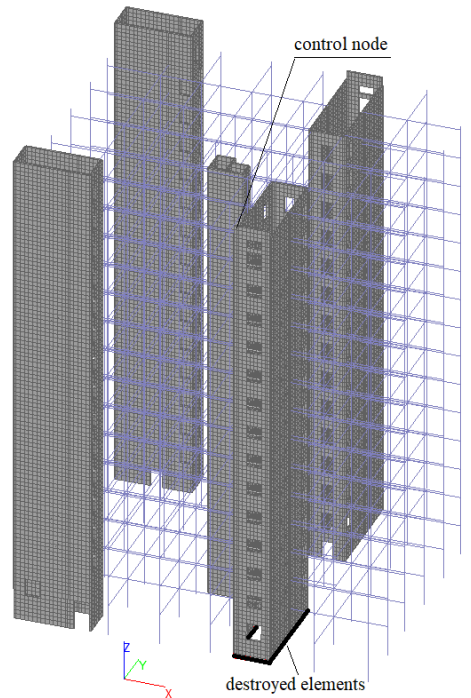
FIG. 12. Design model of the multi-story building without external walls (910 176 equations). The floor slabs are hidden.

load additionally the intact structural elements of the structure. The effectiveness of this approach is outlined in [40–43]. In this paper, we consider the effect of load-bearing walls on improving the reliability of a building in the event of local instantaneous removing of the staircase-elevator block elements. Note that the presented calculation models consist entirely of nonlinear finite elements.

4.1. Example 5

The calculation model is taken from the collection of SCAD Soft[1] problems and is shown in Fig. 12, with floor slabs not shown in order not to obscure the pattern.

The materials used for columns, staircase-elevator blocks, and floor slabs are reinforced concrete. There are no load-bearing walls, except for fragments of the staircase-elevator blocks, which is a typical design solution for buildings of this type. Real design models comprise a lot of structural elements; therefore,

---

[1]SCAD Soft – a software company that develops SCAD Office – a finite element software for structural analysis and design (www.scadsoft.com), certified in accordance with regional norms and one of the most popular software packages used in Ukraine and Commonwealth Independent States (CIS) countries.

we do not provide their parameters. First, the dead load, as well as the live load, is statically applied to the structure. The nonlinear static problem (28) is then solved, and the initial conditions are determined. Second, when solving the Cauchy problem (27), all finite elements in the bottom row of the staircase-elevator block are suddenly removed (Fig. 12). As a result of this, the static equilibrium of the system is disturbed, and the structure fragments begin to move. We limit ourselves to removing only one row of finite elements since removing several rows will not fundamentally change anything. The finite elements of the bottom row are selected since they are the most heavily loaded.

Figure 13 shows the vertical displacement of the controlled node (Fig. 12) over time, and Fig. 14 – the subsidence of the damaged staircase-elevator block together with the adjacent floor slabs.
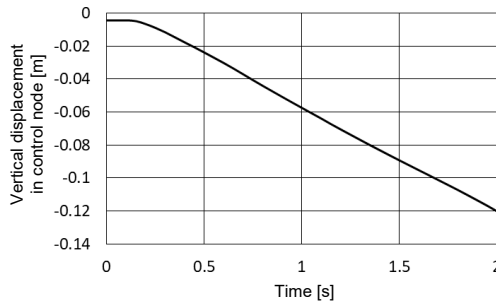

FIG. 13. Vertical displacements in the control node [m].
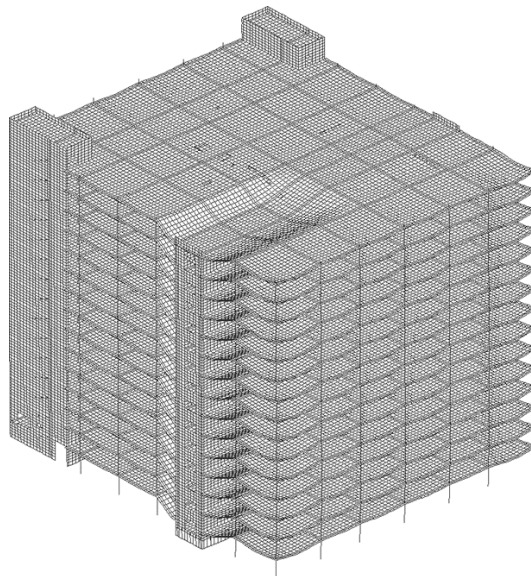
FIG. 14. Subsidence of the damaged staircase-elevator block.

The nature of the movements of the controlled node (Fig. 13) indicates that there is an unlimited increase in displacements – a progressive collapse of the structure occurs. To estimate the state of finite elements, we use the terms "damaged" and "destroyed". Damaged finite elements are those in which at least one of the following events has occurred: the beginning of yielding of the reinforcement in the tension and/or compression zone, or the concrete reaching the yield point in the compressed zone (Fig. 1, point D) at least one Gaussian point. Destroyed finite elements are those in which the maximum deformation of the reinforcement in the tensile or compressed zones has been exceeded (rupture of the reinforcement) and/or the maximum deformation of the concrete in the compressed zone has reached at least one Gaussian point (Fig. 1, point F).

Figure 15 shows damaged and destroyed finite elements, and most of the marked floor slabs have ruptured in the reinforcing rods and there is destruction of concrete not only in the tension zone, which is natural during the normal exploitation of reinforced concrete but also in the compressed zone.
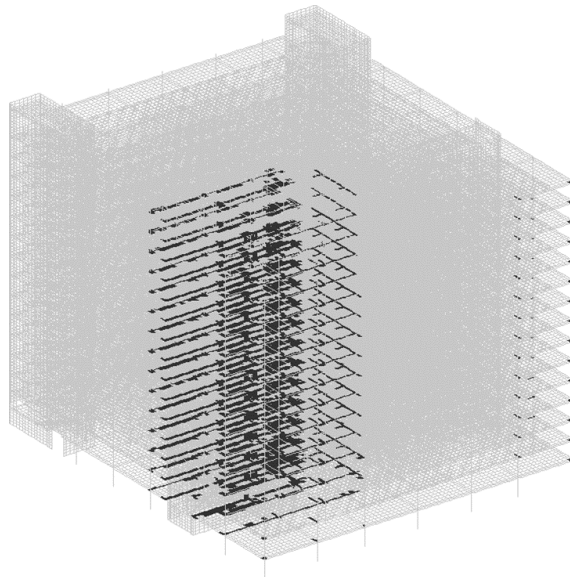

Fig. 15. Damaged and destroyed finite elements.

This problem was solved on the computer specified in Subsec. 3.4 with a 12-core Intel Core i9 processor with 12 threads. The total solution time is 45002 s (12 h 5 min 2 s), the parallel assembly of the tangent stiffness matrix is 17725 s, its factorization – 14889 s, calculation of the residual vector – 7273 s, direct and back substitutions – 2159 s. The integration step was $\triangle t = 0.0005$ s, 3000 steps, and 6029 iterations of the Newton–Raphson method were performed.

4.2. Example 6

The calculation model is presented in Fig. 16 and is obtained from the previous one by adding external load-bearing walls.
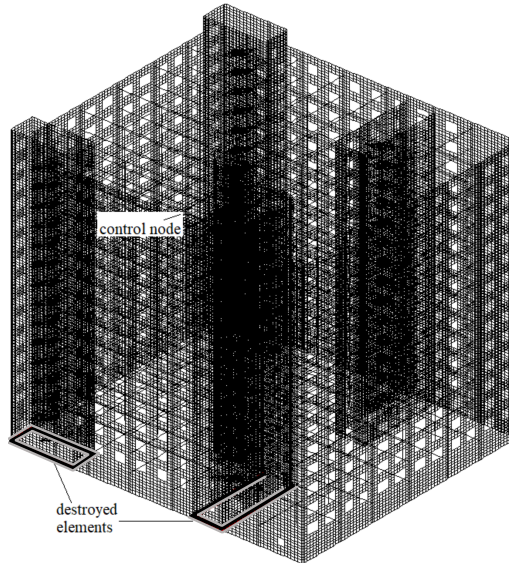

FIG. 16. Design model of a multi-story building with external walls (1 027 082 equations). The floor slabs are hidden.

The remaining parameters are assumed to be the same as in the previous design model. The destruction scenario is that after the application of a static load (dead and live loads), the finite elements of the bottom rows of two staircase-elevator blocks are instantly removed (Fig. 16). The control node is taken as in the previous case: the top corner node of the right staircase-elevator block.

As in the previous case, the nonlinear statics problem (28) is first solved, after which the displacements and states of the finite elements are taken as initial conditions for solving the Cauchy problem (27). Figure 17 shows the vertical displacements of the same control node as in the previous design model. Even though the lower parts of two staircase-elevator blocks are now being removed at once, the vertical displacement of the control node is limited in time, which indicates the absence of progressive destruction. This problem was solved on the computer specified in Subsec. 3.4 with a 12-core Intel Core i9 processor and 12 threads. The total solution time is 23287 s (6 h 28 min 7 s). The parallel assembly of the tangent stiffness matrix is 7708 s, its factorization is 10673 s, calculation of the residual vector – 2536 s, direct and back substitutions – 2629 s. The integration step is $\triangle t = 0.0005$ s, 1500 steps, and 2029 iterations of the Newton–Raphson method were performed.
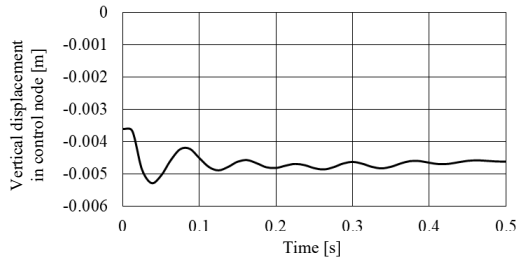
F<small>IG</small>. 17. Vertical displacements in the control node [m].

5. Conclusions

This paper proposes a method for analyzing progressive collapse in buildings and structures, based on finite element dynamic analysis of the design model, behavior during the sudden removal of finite elements selected according to an accepted scenario. In contrast to known methods for initiating progressive collapse, based on zeroing the reactions of removed finite elements at given times, the developed approach uses the implicit integration method for the Cauchy problem and avoids contributions from removed finite elements to the tangential stiffness matrix and the vector of internal forces. This approach is much more convenient than the classical one, since it does not require any a priori information about the magnitude of the reactions of the elements being removed, and it can be applied not only to the removal of columns but also to fragments of load-bearing walls and staircase-elevator blocks.

The use of an elastoplastic material model, taking into account the damage-ability of concrete and reinforcement when limiting deformations are exceeded, as well as taking into account geometric nonlinearity, made it possible to obtain an agreement acceptable for engineering practice with the results of various experiments, which substantiates the reliability of the results obtained as well as reliability of the proposed spatial frame and shell finite elements.

Multi-threaded parallelization of the leading procedures for the numerical integration of the Cauchy problem, to which the problem under consideration is reduced, ensures stable acceleration of the method as the number of threads increases up to the number of physical processor cores when solving large problems (Subsec. 3.4). This confirms the effectiveness of the proposed parallelization algorithms and ensures acceptable analysis time (Subsecs. 4.1 and 4.2). For the example shown in Subsec. 3.4, an 8x speedup was achieved on a computer with a 12-core Intel Core i9 SMP architecture compared to solving the same problem on a single thread.

In the vast majority of studies devoted to progressive destruction, this process is modeled based on certain formulations of problems, physical and mechanical

models of the material, destruction scenarios, etc. But, as a rule, no design solutions are considered to increase the resistance of structures to progressive collapse. Namely, these measures are essential for increasing the survivability of buildings and structures. In [40] and other publications, it was demonstrated that the use of an outrigger floor significantly increases a building's resistance to progressive collapse. This paper shows that the use of load-bearing external walls in addition to columns and staircase-elevator blocks also significantly increases the survivability of the building. In both cases, the same type of calculation models were considered, in which the vertical load-bearing elements were columns and staircase-elevator blocks.

The presented method is aimed at modeling the initial behavior of structures after the instantaneous removal of selected finite elements. If the movement of structural elements is oscillatory (Figs. 9 and 17), then the initial destruction is localized, and no progressive collapse occurs. If the movement of structural elements is aperiodic with displacements increasing over time (Fig. 13), then the destruction of structural elements progresses. Thus, the nature of the movement of structural elements serves as a natural criterion for determining whether progressive collapse has begun or not. To expand the limits of applicability of the method for displacement values comparable to the height of the floor, it is necessary to take into account the change in the initial geometry of the structure, updating the coordinates of the nodes at the end of each converged step of nonlinear iterations, and also take into account the fall of debris on the floors located below, which is one of possible directions for further development of the method.

Another prospects for the future development of the proposed method, according to the author's vision, are as follows. The presented method and algorithms, without fundamental changes, can be used for both nonlinear seismic analysis of buildings and structures, and for the analysis of the assembly of structures, taking into account both geometric and physical nonlinearity. This is possible because the proposed approach allows not only to remove finite elements from the calculation model, but also for their addition. Moreover, it is possible to implement not only the sudden removal of certain elements but also their gradual removal over a given time interval, without having any a priori information on the stress-strain state of these elements.

References

1. Z.P. Bazant, J.L. Le, F. Greening, D.B. Benson, *Collapse of World Trade Center towers: What did and did not cause it?*, Structural engineering Report No, 07-05/C605c, Department of Civil and Environmental Engineering Northwestern University Evanston, Illinois, USA, 2007, https://www.researchgate.net/publication/_Collapse_of_world_trade_center_towers_what_did_and_did_not_cause_it.

2. F. Kiakojouri, M.R. Sheidaii, V. De Biagi, B. Chiaia, Progressive collapse of structures: A discussion on annotated nomenclature, *Structures*, **29**: 1417–1423, 2021, doi: 10.1016/j.istruc.2020.12.006.

3. J.M. Adam, F. Parisi, J. Sagaseta, X. Lu, Research and practice on progressive collapse and robustness of building structures in the 21st century, *Engineering Structures*, **173**: 122–149, 2018, doi: 10.1016/j.engstruct.2018.06.082.

4. H. Wang, A. Zhang, Y. Li, W. Yan, A review on progressive collapse of building structures, *Open Civil Engineering Journal*, **8**: 183–192, 2014, https://opencivilengineering journal.com/contents/volumes/V8/TOCIEJ-8-183/TOCIEJ-8-183.pdf.

5. L. Kwasniewski, Nonlinear dynamic simulations of progressive collapse for a multi-story building, *Engineering Structures*, **32**: 1223–1235, 2010, doi: 10.1016/j.engstruct.2009.12.048.

6. F. Fu, 3-D nonlinear dynamic progressive collapse analysis of multi-storey steel composite frame buildings – Parametric study, *Engineering Structures*, **32**: 3974–3980, 2010, doi: 10.1016/j.engstruct.2010.09.008.

7. J. Li, H. Hao, Numerical study of structural progressive collapse using substructure technique, *Engineering Structures*, **52**: 101–113, 2013, doi: 10.1016/j.engstruct.2013.02.016.

8. S. Kokot, A. Anthoine, P. Negro, G. Solomos, Static and dynamic analysis of a reinforced concrete flat slab frame building for progressive collapse, *Engineering Structures*, **40**: 205–217, 2012, doi: 10.1016/j.engstruct.2012.02.026.

9. S. Kokot, Response spectrum of a reinforced concrete frame structure under various column removal scenarios, *Journal of Building Engineering*, **49**: 103992: 1–17, 2022, doi: 10.1016/j.jobe.2022.103992.

10. F. Sadek, J.A. Main, H.S. Lew, Y. Bao, Testing and analysis of steel and concrete beam-column assemblies under a column removal scenario, *Journal of Structural Engineering*, **137**(9): 881–892, 2011, doi: 10.1061/(ASCE)ST.1943-541X.0000422.

11. B.A. Izzuddin, A.G. Vlassis, A.Y. Elghazouli, D.A. Nethercot, Progressive collapse of multi-storey buildings due to sudden column loss — Part I: Simplified assessment framework, *Engineering Structures*, **30**: 1308–1318, 2008, doi: 10.1016/j.engstruct.2007.07.011.

12. E. Stoddart, M. Byfield, B. Davison, A. Tyas, Strain rate dependent component based connection modelling for use in non-linear dynamic progressive collapse analysis, *Engineering Structures*, **55**: 35–43, 2013, doi: 10.1016/j.engstruct.2012.05.042.

13. A. McKay, K. Marchand, M. Diaz, Alternate path method in progressive collapse analysis: variation of dynamic and nonlinear load increase factors, *Practice Periodical on Structural Design and Construction*, **17**(4): 152–160, 2012, doi: 10.1061/(ASCE)SC.1943-5576.0000126.

14. M. Liu, A new dynamic increase factor for nonlinear static alternate path analysis of building frames against progressive collapse, *Engineering Structures*, **48**: 666–673, 2013, doi: 10.1016/j.engstruct.2012.12.011.

15. J. Mashhadi, H. Saffari, Dynamic increase factor based on residual strength to assess progressive collapse, *Steel and Composite Structures*, **25**(5): 617–624, 2017, doi: 10.12989/scs.2017.25.5.617.

16. O.A. Mohamed, Calculation of load increase factors for assessment of progressive collapse potential in framed steel structures, *Case Studies in Structural Engineering*, **3**: 11–18, 2015, doi: 10.1016/j.csse.2015.01.001.

17. M. Ferraioli, Dynamic increase factor for nonlinear static analysis of RC frame buildings against progressive collapse, *International Journal of Civil Engineering*, **17**(3): 281–303, 2019, doi: 10.1007/s40999-017-0253-0.

18. S.Yu. Fialko, Application of finite element method to analysis of strength and bearing capacity of thin-walled concrete structures, taking into account the physical nonlinearity [in Russian], ASV, SCAD Soft, Moscow, 2018.

19. *CSI Analysis Reference Manual* (last access 11.07.2024), Computers & Structures, Inc., Berkeley, CA, USA, https://docs.csiamerica.com/manuals/sap2000/CSiRefer.pdf.

20. E.L. Wilson, *Three-Dimensional Static and Dynamic Analysis of Structures*, 3rd ed., Computers and Structures, Inc., Berkeley, CA, USA, 2002.

21. G.A. Geniev, V.N. Kissyuk, G.A. Tyupin, *The Theory of Plasticity of Concrete and Reinforced Concrete* [in Russian], Stroyizdat, Moscow, 1974.

22. M.A. Criesfield, *Non-linear Finite Element Analysis for Solids and Structures*, Vol. 1, Essentials, John Wiley & Sons, Chichester, New York, 2000.

23. S. Fialko, Quadrilateral finite element for analysis of reinforced concrete floor slabs and foundation plates, *Applied Mechanics and Materials*, **725−726**: 820–835, 2015, doi: 10.4028/www.scientific.net/AMM.725-726.820.

24. S.Yu. Fialko, Dynamic analysis of the elasto-plastic behaviour of buildings and structures in the SCAD++ software package, *Journal of Physics: Conference Series*, **1425**: 012041, 2019, doi: 10.1088/1742-6596/1425/1/012041.

25. K.J. Bathe, *Finite Element Procedures*, Prentice Hall, New Jersey, 1996.

26. K.U. Bletzinger, M. Bischoff, E. Ramm, A unified approach for shear-locking-free triangular and rectangular shell finite elements, *Computers & Structures*, **75**: 321–334, 2000, doi: 10.1016/S0045-7949(99)00140-6.

27. IntelMKL Resource & Documentation Center (last access 22.01.2023), https://www.intel.com/content/www/us/en/develop/documentation/onemkldeveloper-reference-c/top.html.

28. T.J.R. Hughes, T. Belytschko, Nonlinear finite element analysis, Course Notes, September 4–8, Munich, Germany, 1995.

29. I. Miranda, R.M. Ferencz, T.J.R. Hughes, An improved implicit-explicit time integration method for structural dynamics, *Earthquake Engineering and Structural Dynamics*, **18**: 643–653, 1089, doi: 10.1002/eqe.4290180505.

30. S. Fialko, Parallel finite element solver for multi-core computers with shared memory, *Computers and Mathematics with Applications*, **94**: 1–14, 2021, doi: 10.1016/j.camwa.2021.04.013.

31. S. Fialko, Parallel algorithms for forward and back substitution in linear algebraic equations of finite element method, *Journal of Telecommunications and Information Technology*, **4**: 20–29, 2019, doi: 10.26636/jtit.2019.134919.

32. S.Yu. Fialko, V.S. Karpilowskyi, Triangular and quadrilateral flat shell finite elements for nonlinear analysis of thin-walled reinforced concrete structures in SCAD software, [in:] W. Pietraszkiewicz, W. Witkowski [Eds.], *Shell Structures: Theory and Applications*, Vol. 4, pp. 367–370, CRC Press Taylor & Francis Group, London, New York, 2017, doi: 10.1201/9781315166605-83.

33. S. Fialko, V. Karpilovskyi, Spatial thin-walled reinforced concrete structures taking into account physical nonlinearity in SCAD software. Rod finite element, [in:] *13th International Conference Modern Building Materials, Structures and Techniques*, May 16–17, pp. 728–735, Vilnius Gediminas Technical University, 2019, doi: 10.3846/mbmst.2019.086.

34. A.V. Savchenko, A.V. Ioskevich, L.F. Khazieva, A.A. Nesterov, V.V. Ioskevich, Solution of the longitudinal and transverse bending beam in different software package, *Construction of Unique Buildings and Structures*, **38**(11): 89–105, 2015, doi: 10.18720/CUBS.38.7.

35. A.S. Vol'mir, *Stability in Deformable Systems* [in Russian], Fizmatgiz, Moscow, 1967.

36. J. Němeček, P. Padevět, B. Patzák, Z. Bittnar, Effect of transversal reinforcement in normal and high strength concrete columns, *Materials and Structures*, **38**(7): 665–671, 2005, doi: 10.1007/BF02484311.

37. J.M. Adam, M. Buitrago, E. Bertolesi, J. Sagaseta, J.J. Moragues, Dynamic performance of a real-scale reinforced concrete building test under a corner-column failure scenario, *Engineering Structures*, **210**: 104414, 2020, doi: 10.1016/j.engstruct.2020.110414.

38. A.V. Perelmuter, V.I. Slivker, *Numerical Structural Analysis*, Springer, Berlin, Heidelberg, 2003, doi: 10.1007/978-3-540-36500-6.

39. S.Yu. Fialko, Application of rigid links in structural design models, *International Journal for Computational Civil and Structural Engineering*, **13**(3): 119–137, 2017, doi: 10.22337/1524-5845-2017-13-3-119-137.

40. S.Yu. Fialko, O.V. Kabantsev, A.V. Perelmuter, Elasto-plastic progressive collapse analysis based on the integration of the equations of motion, *Magazine of Civil Engineering*, **102**(2): 10214, 2021, doi: 10.34910/MCE.102.14.

41. O.A. Mohamed, O. Najm, Outrigger systems to mitigate disproportionate collapse in building structures, *Procedia Engineering*, **161**: 839–844, 2016, doi: 10.1016/j.proeng.2016.08.725.

42. M. Ferraioli, A. Lavino, A. Mandara, Progressive collapse assessment and retrofit of a multistory steel braced office building, *International Journal of Steel Structures*, **22**(4): 1086–1107, 2022, doi: 10.1007/s13296-022-00626-x.

43. F. Freddi, L. Ciman, N. Tondini, Retrofit of existing steel structures against progressive collapse through roof-truss, *Journal of Constructional Steel Research*, **188**: 107037, 2022, doi: 10.1016/j.jcsr.2021.107037.